Nodal Integral Method for Convection-Diffusion transport in complex domain using linear and higher order quadrilateral elements

A Dissertation Submitted
in partial fulfilment of the requirements
for the degree of

Master of Engineering
in
Thermal Engineering

by

Rishabh Prakash Sharma

Registration No.: 801583021

Under the supervision of

Dr. Neeraj Kumar

Assistant Professor

MECHANICAL ENGINEERING DEPARTMENT

THAPAR UNIVERSITY, PATIALA

July, 2017

CERTIFICATE

I hereby declare that the thesis entitled, **"Nodal Integral Method for Convection-diffusion transport in complex domain using linear and higher order quadrilateral elements"** is an authentic record of my work carried out as per requirements for the award of degree of **Master of Engineering** in **Thermal Engineering** at **Thapar University, Patiala** under the supervision of **Dr. Neeraj Kumar**, Assistant Professor, Mechanical Engineering Department, Thapar University, Patiala during July 2015 to July 2017. No part of the matter embodied in this report has been submitted to any other university or institute for the award of any other degree.

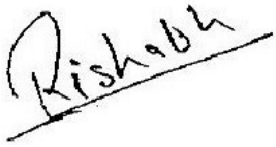

Date: 17/07/2017 **Rishabh P Sharma**

It is certified that the above statement made by the student is correct to the best of my knowledge and belief.

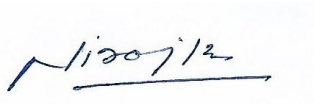

Dr. Neeraj Kumar

Assistant Professor

Mechanical Engineering Department

Thapar University, Patiala - 147004

Dedicated to

Science & Humanity

Acknowledgements

I would like to express my sincere gratitude to my supervisor **Dr. Neeraj Kumar, Assistant Professor, Mechanical Engineering Department, Thapar University, Patiala** for the continuous support of my ME research work. His office doors were always open for me whenever I have any doubt either related to my research work or my career. He help me a lot in learning process of new tools related to computational work. During my tenure, he contributed to a rewarding graduate school experience by giving me intellectual freedom in my work, engaging me in new ideas, and demanding a high quality of work in all my endeavors. Thank you for having faith in me.

Additionally, I would also like to thank **Prof. Neeraj Grover** , for helping me to learn shape functions and transformation used in my thesis work. He is an extremely reliable source of FEM. I was fortunate enough to work with him.

Least but not last, I would like to thank my friends and my family, who have supported me throughout entire process, both by keeping me harmonious and helping me putting pieces together. I will be grateful forever for your love.

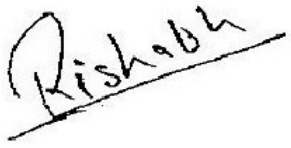

Rishabh Prakash Sharma

Abstract

Generic nodal integral method (NIM) based scheme, utilizing nine noded 2D quadratic elements along with four noded 2D linear elements, is developed to solve the fluid flow and heat transfer equations in complex geometries. Non-linear (quadratic) quadrilateral elements are used for discretization of boundary region and linear quadrilateral elements are used for interior region. Lagrange interpolation functions are used to map both type of elements to corresponding square computational elements. The scheme for Neumann and mixed type of boundary conditions are also developed for quadratic elements. C-1 type continuity condition is imposed at the interfaces of adjacent elements. Numerical results are compared with analytical solutions for diffusion and advection-diffusion equations. Results for Navier-Stokes equations in curved domain are compared with previously reported experimental as well as numerical results. The comparative study has also been done between presently developed scheme using quadratic and linear elements (referred as scheme-1) and scheme based on complete discretization with linear elements (referred as scheme-2). The comparison shows that scheme-1 is more accurate than scheme-2 while the order of accuracy is same for both the schemes. The results show that the efficient mapping of curved surface with quadratic elements improves the accuracy of NIM schemes.

Key words: Nodal Integral Method, Convection-diffusion equation, Navier-Stokes equations, Coarse mesh methods.

Contents

List of Figures

List of Tables

Nomenclature

α	Thermal Diffusivity
α_ξ	Redefined diffusivity of transformed CDE
$\bar{T}^\eta$	η averaged temperature in local coordinate system
$\hat{T}$	Temprature in global coordinate system
∇^2	Laplace operator
ξ_x	First order derivatives with respect to x
ξ_{xx}	Second order derivatives with respect to x
ζ	Local Coordinate System (ξ, η)
A_i	Coefficient of 3-point scheme in ξ direction
B_i	Coefficient of 3-point scheme in η direction
C^i	Order of continuity
C_i	Coefficient for x coordinate
D_i	Coefficient for y coordinate
Fij	Coefficient of final discrete equation
K_i	Integral constants
m_x	Direction cosines in x direction
m_y	Direction cosines in y direction
N_i	Shape functions
T	Temprature in local coordinate system
T_p	Point values of temperature
u	Velocity component in x direction

u_c Redefined velocity terms of transformed CDE

v Velocity component in y direction

$\bar{S}^{\xi\eta}$ Cell averaged Pseudo-Source term

$\hat{\xi}$ Global Coordinate System (x, y)

J Jacobian Matrix

M&C Coefficient Matrix

Abbreviations

CDE Convection Diffusion Equation.

FDM Finite Difference Method.

FVM Finite Volume Method.

JFKM Jacobian Free Newton Krylov Method.

MNIM Modified Nodal Integral Method.

MPI Message Passing Interface.

NGFM Nodal Green Function Method.

NI-FAM Nodal Integral-Finite Analytic Method.

NI-FEM Nodal Integral-Finite Element Method.

NIM Nodal Integral Method.

ODE Ordinary Differential Equation.

PDE Partial Differential Equation.

QUICK Quadratic Upstream Interpolations for Convective Kinectics.

SIMPLE Semi Implicit Method based Pressure Linked Equations.

SOU Second Order Upwinding.

TIP Transverse Integration Procedure.

Chapter 1

Introduction

1.1 Introduction

Solving the governing equations for fluid flow and heat transfer physics in complex geometries are still a computationally expensive task. Well established numerical methods like FVM and FDM still need very fine grids to resolve these physics. Numerical solutions for fluid flow equations in complex geometries are usually obtained by using more refined grids. Thus, a numerical method that can yield better results on a coarse mesh, is desirable.

Nodal integral methods (NIM) are known for giving reasonably accurate numerical results over relatively coarser grids in various physics [2, 3]. Initially, it is developed for solving Neutron diffusion equation in reactor physics [4]. Later it is extended to solve fluid flow equations [5]. NIM has established itself as an efficient method to solve the governing equations numerically in regular Cartesian domains (formed by the union of rectangular nodal cells) [2, 3, 6–15]. However, for complex domains, more refinement of these rectangular cells at curved boundaries adversely affects the coarse grid accuracy of NIM. There are also certain limitations of applicability of this method in the irregular or complex domains due to local transverse integration procedure (TIP). TIP is a unique procedure applied in NIM over a local discrete cell to generate cell analytical solution. This procedure requires that the local cell should be fitted in the regular Cartesian coordinate system. These limitations are eased to some extent by developing nodal methods for cylindrical geometries [2, 10, 14] and hexagonal geometries [9]. However, the applicability of NIM in arbitrary-shaped geometries is still limited and only applied to boundary-fitted orthogonal coordinate system [15]. To overcome the above-mentioned limitations, Toreja and Rizwan-uddin [6] have proposed hybrid methods for fluid flow problems. These hybrid methods, NI-FEM and NI-FAM, are developed by using finite element method (FEM) and finite analytic method (FAM) respectively along with NIM. Although both the hybrid methods are developed to relax the geometry restrictions of computational domains, they are still limited to regular Cartesian grids. In another approach, Nezami et al. [8] have used iso-parametric transformation to conquer the geometry restriction of NIM. These alge-

braic transformation map an arbitrary shaped quadrilateral element into a square element. NIM scheme using this bi-linear transformation is further improved by Kumar et al. [13] by including cross-derivative terms which are neglected in previous schemes. The scheme for Neumann type boundary condition is also developed to increase the applicability of these schemes in various physical situations.

In the current work, NIM scheme is developed for non-linear quadrilateral elements. Both *nine* noded quadratic and *four* noded linear quadrilateral elements are used in discretization procedure. Quadratic elements are used to discretize the region of curved boundaries and linear quadrilateral elements are used for interior of the domain. Bi-quadratic Lagrange interpolation is used to map the quadratic elements and Bi-linear interpolation is used to map the linear elements into the corresponding local square elements. This approach enhances the flexibility of NIM scheme for its application in complex domain. Moreover, a novel approximate discretize scheme for implementation of boundary conditions on the curved surfaces is also developed. This is done by piecewise linearization of curved boundary for both Neumann and mixed type of boundary conditions.

Developed scheme using the combination of linear and quadratic quadrilateral elements applied to solve diffusion, advection-diffusion and Navier-Stokes equations in curved domains. For linear problems, numerical results are compared with analytical solutions and for non-linear problems (N-S equations) results are compared with experimental as well as fine grid numerical solutions [1]. The applicability of the NIM scheme for Dirichlet as well as Neumann boundary conditions is also tested in the test cases. The comparative study between the scheme utilizing linear and quadratic elements with the scheme based on complete linear discretization has been done in this article. This study reveals that the accuracy of the scheme get enhanced by 15-20% when quadratic cells are used in discretization of boundary along with linear discretization of interior of domain.

1.2 Literature Survey

Nodal integral method is developed on the basis of transverse averaging which is a unique procedure of nodal methods. Many researcher modified the nodal methods, resulting various form of these methods as modified NGFM, NIM, MNIM, NIFEM, NIFAM and many other methods are evolved from these nodal methods. Their works and findings have been briefly summarized below:

1. **Fischer and Finnemann [4]** have developed a analytic nodal method, NIM, to solve the three dimensional, coupled neutron diffusion equations. Transverse averaging of leakage shapes were done in terms of parabolas which was the only approximation in this approach. To determine the coefficient's of parabola, two different methods were used in this article. This method, NIM, was tested and verified against bench mark solutions of neutron diffusion equation. Nodal integral method (NIM) yields another diverse solver, besides NEM, which is well known in nuclear industry. Both the solvers NIM and NEM were used in same iteration manner so that they can easily be exchanged in reactor core simulator. This resulting a diverse solver for on-site use in plant control systems.

2. **Lawrence and Dorning [16]**, have developed a nodal method to solve the multidimensional neutron diffusion equation. This method was based upon the linear form of nodal balance equation. These nodal balance equations was defined in terms of average partial currents over the surface of node. A set of coupled 1-D integral equations, which were defined over the local discrete sub-domains, was generated using Green's functions. Transverse integrating procedure, reduced the multidimensional neutron diffusion equation to the coupled set of one-dimensional ordinary differential equations which were obtained over the transverse directions. Resulting, integral equations were exact solutions defined over a nodal cell. Furthermore, these integral equations were approximated with weighted residuals within each nodal cell. This approximation leads to matrix equations, which were solved with linear nodal balance equation. The said nodal balance equations provide additional relationship between the flux within the node and interface of partial currents. The developed method was tested with a four-group liquid-metal fast breeder reactor problem and also with 2D and 3D light water reactor benchmark problems. The obtained results shows the capability of nodal methods which can generate very accurate results with significant smaller computing time in comparison to the standard finite difference methods (FDM).

3. **Azmy and Dorning [17]**, For steady state flow problems (Navier-Stokes), Nodal integral method (NIM) was developed. However, the NIM method was still based on the traditional transverse averaging procedure (TIP), the method was different from the previous nodal green function method (NGFM) because of less number of unknown for a dependent variable. Thus due to lack of complexity, NIM was much easily used in complex

problems. The developed scheme was tested with various fluid flow (Flow between parallel plates and Lid driven cavity) and heat transfer (Boussinesq approximation for natural convection) problems. On verification of NIM scheme with benchmark solutions, It was concluded that the scheme is quite accurate on relatively coarse grids.

4. **Horek and Dorning [18]** have developed an efficient a nodal method using transverse integration procedure for incompressible laminar flow physics. Local Green's tensors were also introduced in transverse averaged Navier-Stokes equations and continuity equations. This scheme was tested with various 2D test cases including inlet flow, fully developed flow, modified driven cavity problems with inlet and outlet sections. The nodal Green's tensor method showed very high accuracy, which lead to a efficient computational method with quite coarse grid sizes. However, the main disadvantage of this methodology is that, it produces more unknown for a dependent variable. Thus complexity of this method is still a disadvantage in comparison to NIM scheme.

5. **Azmy, Y.Y. [2]** have further modified the existing nodal methods and developed a nodal integral method (NIM) for solving the neutron diffusion equation in cylindrical geometry. Since the traditional nodal methods were restricted to rectangular computational domains, this modification increase the applicability of nodal method over complex curvilinear geometry. The developed numerical scheme was tested with two problems which were obtained by Exterminator-2 code. The results shows that nodal integral method is computationally efficient and requires less CPU times in comparison to the usual finite difference methods (FDM) and finite element methods (FEM). However the developed nodal scheme and set of final discrete equations are more complicated than the other conventional counterparts.

6. **Hennart, J.P. [19]** In this article, basis numerical analysis has been done of nodal analytical methods, which were originally developed for nuclear reactor problems and further extended for numerical solution of PDEs. The discretization of problem domain was done using the regular nodal cells. In this article transverse integration for a independent variable was used for parent PDE which leads to a set of 1D-ODEs for that independent variable. These ODEs were solved analytically, using particular integral method as well as other fundamentals. After the thorough analysis of existing analytical methods, an extended analytical methodology was proposed. The conclusions were made on behalf

of super convergence results with respective particular scheme.

7. **Wilson et al. [20]**have developed two new nodal integral methods: one, lower order and other one was with higher order to solve the time-dependent. incompressible natural convection problem. Both of the methods were higher level accurate even with large grid size and have the ability to produce results independent of Courant condition. The results were generated for different test cases: one, double-gazing, to verify the accuracy in space time and other, bifurcation searches and stability of flow regions. These test cases showed the ability of NIM scheme to duplicate the natural phenomena without bifurcation points, turning points and spurious solutions. compared with the benchmark problems. The developed schemes were also used to examine the critical aspect ratio at which the alternative stable solutions can be obtained from a no-flow condition.

8. **Michael et al.[21]** Third order nodal integral method was developed in this article. The previously reported second order nodal method was reviewed in this article for development and comparison of third order NIM. The linear part of pseudo-source terms which appear in transversely integrated equations was approximated by introducing upwind approximation. This approximation was introduced in NIM scheme. In the traditional NIM methodology, additional equations are required for closer form of scheme formulation. This tradition was obviated by introducing upwind approximation NIM scheme. The second-order nodal scheme and the third order NIM which has two version: one, full third order nodal method and the other, which used second order equations near the boundaries were compared with recently developed state-of-the-art method and other traditional methods. The comparative study showed that among the studied five methods, second-order NIM scheme has highest computational efficiency with 1% error.

9. **Rizwan Uddin [22]** NIM was developed for one dimensional advection-diffusion equation. This NIM scheme was based on the nodal approach and results second order numerical scheme for both space and time variables. This scheme showed inherent-upwinding and can be further extended to multidimensional problems. Coupling of nodal scheme with interior reconstruction of the solution results a powerful numerical scheme that can resolve the regions with sharp gradients even with relatively coarse grid. Three test cases of convection-diffusion equation were solved using the developed NIM scheme to demonstrate the accuracy of scheme.

10. **Rizwan Uddin [23]** have modified the existing nodal integral method to solve the PDEs. In this modification nonlinear terms or so called pseudo-source terms were treated by approximating the part of non-linear terms of discrete field variables instead of whole pseudo-source terms. Remaining part or complete pseudo-source terms of transverse-integrated equations were kept left-hand side and to be solved analytically. This modification reduced the complexity of method and also give closure form of formulation process. This modified NIM was tested with Burger equation which lead to exponential variation of field variable within the nodal cell. Resulting scheme for Burger equation showed inherent upwinding due to exponential terms. Transverse integration procedure (TIP) for a independent variable reduce a PDE as a function of that independent variable, averaged in all other directions. This TIP allows NIM to obtain accurate results even on coarse grid. The obtained numerical result were compared with the results of other contemporary methods. The comparative study showed that the developed new method was comparable and sometimes generates better results then the currently used schemes. These schemes can be further extended to multidimensional and time-dependent problems.

11. **Toreja and Rizwan [6]**have developed two hybrid numerical schemes. NI-FAM was developed using nodal-integral method with finite analytic method (FAM) and NI-FEM was developed using NIM with finite element method (FEM). Both the schemes were developed to solve two-dimensional, time-dependent as well as steady-state convectiondiffusion equation (CDE). The computational domain was discretized using rectangular as well as triangular nodes. Rectangular elements were used for interior of domain as well as vertical and horizontal boundaries. However, the boundaries which were not either vertical or horizontal were discretized using triangular elements. In time-dependent problem, the triangular and rectangular element became space-time wedge and parallelepiped shaped nodes, respectively. At the interface of adjacent rectangular/parallelepiped nodal cell, difference scheme was developed for averaged variables using conventional NIM. In NI-FEM trial function was used for triangular elements. These trial function were made to satisfy the advection-diffusion equation in integral sense and written in terms of edge-averaged concentration of three edges . In NI-FAM, finite analytic approximation was used for representation of the concentration over the wedge/triangular shaped cells. This finite analytic approximation was made by satisfying the analytic solution of

one dimensional CDE. For both the hybrid schemes, difference schemes were developed at the interfaces of triangular/wedge and rectangular/parallelepiped-shaped elements by applying the continuity condition of the flux across interface.

12. **Wang and Rizwan [3]**, developed a novel numerical scheme for time-dependent, incompressible, Navier-Stokes equations coupled with pressure Poisson equations. TIP was applied to these PDEs and converted them to transverse averaged ODEs. These ODEs were in terms of discrete variables pressure and averaged velocities. Furthermore, these ODEs were solved in terms of averaged variables and then utilized to develop the difference scheme. This semi-implicit scheme was developed for brick-like cells and has inherent upwinding. The variation of transverse-averaged pressure was considered quadratic in spatial direction. However the variation of transverse averaged velocity was the sum of a linear term and an exponential term. Delayed coefficients were also utilized in this scheme which leads to one evaluation for each time step. Several test problem were tested and the results showed the robustness of nodal scheme due to second order error. The scheme performed very well and lead to small errors even with large grid sizes.

13. **Nezami et al. [8]** firstly developed the Nodal integral methods (NIMs) for arbitrary shaped quadrilateral elements which relaxed the geometry restriction of NIM schemes. These NIM based schemes were used to solve the various governing equations of different areas of physics. These schemes are powerful numerical schemes which can solve the governing PDEs accurately even with quite coarse grid. However a unique procedure of NIM schemes, transverse averaging procedure (TIP) restricts NIM to solve these PDEs in brick-like cells which limits its application in complex geometries. This limitation was eased out by Nezami et al. [8]. The discretization was done using arbitrary quadrilaterals which increased the applicability of NIM scheme in complex domain. These arbitrary quadrilaterals were transformed to unit square elements by using Lagrange bilinear interpolation function. The governing equations were also transformed to these local square computational domain. Now the transformed PDEs were solved using traditional NIM. This scheme was tested with Poisson equation as well as time-dependent advection-diffusion equations.The generated results were verified with benchmark problems. The results were quite promising and showed that algebraic transformation with

NIM scheme retains its accuracy with coarse grid sizes.

14. **Huang and Rizwan,[24]**, have further developed the work of Nezami et al. [8] for time-dependent, incompressible Navier-Stokes equations. Modified NIM scheme was developed to solve the Navier-Stokes equations in arbitrary shaped domains. Again the four noded elements are used in discretization procedure. Algebraic transformation was used to transform the arbitrary quadrilateral elements into discrete square cells. This algebraic transformation was done using bi-linear Lagrange interpolation function similar to the approach of Nezami et al. [8]. Navier-Stokes equations as well as pressure Poisson equation were also transformed to the local coordinate system. Modified NIM scheme was used to solve the two-dimensional shear-driven cavity problem and the results were compared with the analytical solution. The results were quite promising and showed that accuracy of modified NIM can be maintained using non-rectangular elements. These NIM scheme can be further extended for curved domains

15. **Kumar et al. [11]** developed a pressure correction based algorithm based on NIM methodology to solve the steady-state, 2-D incompressible Navier-Stokes equations. Partial differential equations of different areas of physics have been solved using NIM schemes which show very high accuracy in reasonable coarse grid in comparison to other conventional schemes. Semi-Implicit Method for Pressure-Linked Equations (SIMPLE) like algorithm was used in implementation of the NIM scheme. In this algorithm pressure and velocity correction are used instead of solving exact pressure Poisson equation. The developed scheme is verified and tested against two test problems, natural convection of air in a square cavity and shear-driven cavity. For both the test cases NIM schemes performs very well and the generated results are in good agreement with benchmark solutions even with quite coarse grid size.

16. **Kumar et al. [12]**, developed a generic numerical scheme based on the NIM methodology to solve Advection-diffusion equation in complex domain. Two dimensional arbitrary shaped linear quadrilateral elements were used for discretization of problem domain. Each quadrilateral was mapped to unit square element using Iso-parametric one-one onto mapping. This mapping was done using Lagrange bi-linear interpolation function. Also, a novel numerical scheme was developed for implementation of Neumann and mixed-type boundary condition for arbitrary-shaped boundary. At the interface

of two neighboring discrete elements, continuity condition was explicitly formulated. Testing and verification of developed scheme was also done with analytical solution of Convection-diffusion and Diffusion equation in skewed and curved geometry. The generated numerical results agreed fairly well with analytical results even with reasonably coarser grids. It was concluded that NIM schemes have the capability to produce accurate results with much coarser grids even with curvilinear geometries.

17. **Kumar et al. [13]**, developed a numeric scheme which is similar to the scheme for Convection-Diffusion equation. This scheme was based on Nodal Integral Method (NIM) and developed for solving Navier-Stokes equations in arbitrary shaped domain. Pressure correction based algorithm are used for convergence condition and pressure Poisson equation are solved similar to the Diffusion equation. This pressure Poisson equation replaced the continuity condition and SIMPLE like algorithm was used to ensure the convergence criteria. Two test problem,, Shear-driven cavity and buoyance-driven flows were numerically solved for testing and verification of NIM based scheme. The comparative study was also done and the obtained results were compared with fine mesh solution of previous studies using FVM and similar schemes. It was concluded that NIM based schemes for Navier-Stokes equations have the capability to produce quite accurate results even with quite coarse and non-orthogonal grids.

1.3 Gaps Identified

1. Traditional numerical methods require very fine meshes to obtain the accurate results which leads to higher computational costs. Thus a numerical method is required which yield accurate results with coarse mesh.

2. Nodal integral method is a coarse mesh method which fulfill the above requirement but still restricted to regular computational domain due to its unique transverse integration procedure (TIP).

3. These nodal methods were developed for irregular domains using different type of elements in discretization procedure of the complex and curvilinear domains. NIM schemes still require fine meshes to resolve the curved boundary.

4. Although, the regular geometry restriction of NIM is eased out using linear quadrilateral

elements but the curved boundaries still discretized using linear elements which is not a realistic approach.

5. Most researcher used linear approximation in NIM methodology. This approximation only works with linear elements thus modification is still required in NIM approximations for higher order elements.

6. Currently developed Neumann and mixed type of boundary conditions are used for linear quadrilateral elements even with curved boundaries which include error in numerical solutions. Thus proper implementation of these type of boundary conditions are required.

7. Since, no work is reported regarding the behavior of NIM scheme with biased and non-orthogonal grids. Thus a thorough study is required for using this scheme in complex fluid problems.

1.4 Objective of present work

1. To study the algebraic transformation of *nine* noded quadratic quadrilateral elements along with $four$ noded linear quadrilateral elements.

2. To develop a generic numerical scheme based on NIM methodology for diffusion, convection-diffusion and Navier-stokes equations using both linear as well as quadratic quadrilateral elements.

3. To study the Neumann and mixed type of boundary condition for quadratic quadrilateral elements.

4. To develop a novel NIM based scheme for implementation of Neumann and mixed type of boundary condition for curved surface of a quadratic elements.

1.5 Thesis Outline

The detailed discretization procedure of a complex domain using both linear and quadratic quadrilateral elements is described in Chapter-2. Mathematical formulation of NIM scheme using both type of elements are developed in this chapter. Convection diffusion equation is chosen as model equation and the scheme is developed for convection-diffusion equation. On behalf of the developed scheme, the scheme for diffusion and Navier-Stokes equations are also

developed. In this chapter, a novel NIM based scheme is also develop for implementation of Neumann and mixed boundary condition on the curved surface of quadratic elements.

In the Chapter-3, three test cases are chosen for testing and verification of developed NIM scheme. Different grid sizes are used for solving the governing equations in 2D cylindrical wedge domain. The results generated for diffusion and convection-diffusion equations are compared with analytical solution and also with the results of scheme-2 which uses linear elements in complete discretization of problem. For verification of Navier-Stokes equations, polar lid-driven cavity problem is solved in cylindrical wedge domain. The results for N-S equations are compared with the previous experimental as well as numerical solution of multi-grid finite difference method. Qualitative as well as quantitative comparison of results are also done.

Finally in Chapter 4, main conclusions of present work are presented. This chapter also contains the scope for future work.

Chapter 2

NIM for Higher order elements

NIM methods are explicitly developed by application of a unique transverse averaging procedure (TIP) which generates local cell analytical solutions. These cell analytical solutions are the main cause for coarse grid accuracy of NIM. But this averaging procedure also limits the applicability of NIM to rectangular computational domain. In this present chapter, development of NIM scheme for linear PDEs using higher order elements is discussed to demonstrate the flexibility of NIM based schemes over curved geometries. Rest of the thesis consist applications of NIM based scheme in various linear and non-linear problems. These problems are numerically solved in curved geometries to test the feasibility and accuracy of NIM based scheme. The steps in general procedure of NIM are shown in following Fig. 2.1.

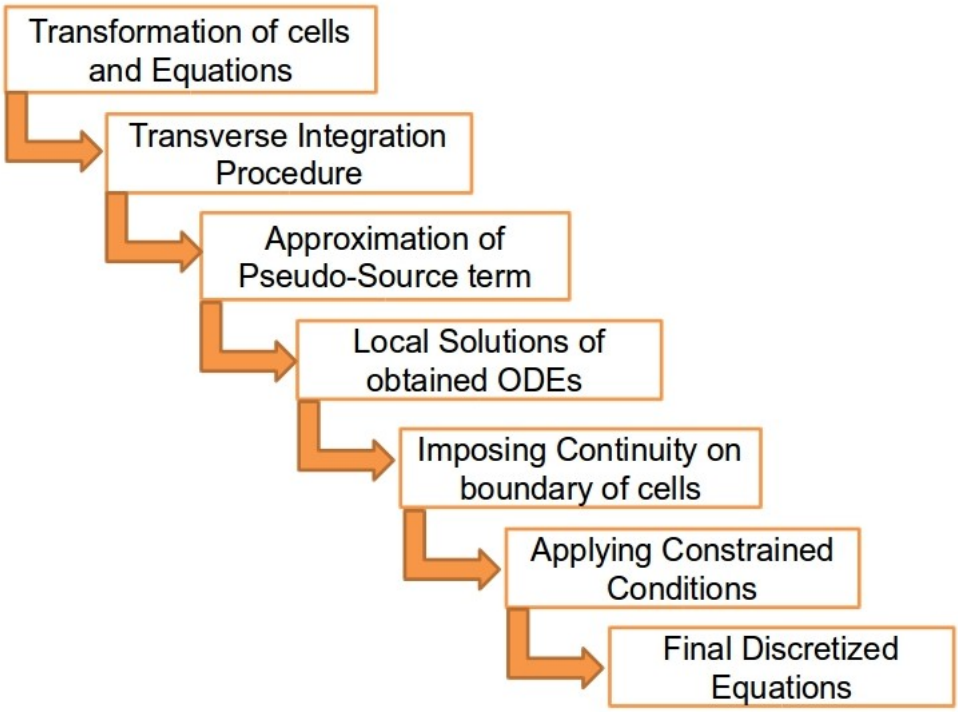

Figure 2.1: Flowchart of NIM methodology

These steps are similar to the previous schemes [8, 13, 23, 25].

2.1 Transformation

The current methodology utilizes linear and quadratic quadrilateral elements to map the arbitrary shaped domain. Each quadratic element has been bijectively mapped using bi-quadratic and each linear element is mapped using bi-linear Lagrangian interpolation functions to corresponding square element. For 2D quadratic quadrilateral element there exist three points on each edge of quadratic cell as shown in Fig. 2.2. The bijective iso-parametrically transformation from global $\hat{\zeta}$ to local ζ domain $f : \mathbb{R}^2 \longrightarrow \mathbb{R}^2$ as follows:

$$P(x,y) = f(Q(\xi,\eta)) \qquad \text{where} \qquad (x,y) = h(\xi,\eta) \tag{2.1}$$

For any continuous function f there $\exists$ a point $\mathbf{Q}(\xi,\eta) \subset \zeta$(local space) for corresponding point $\mathbf{P}(x,y) \subset \hat{\zeta}$(global space), where $\xi,\eta \in [-1,1]$ and $x,y \in \mathbb{R}$. Two dimensional interpolation function for quadratic element is given in Eq. (2.2):

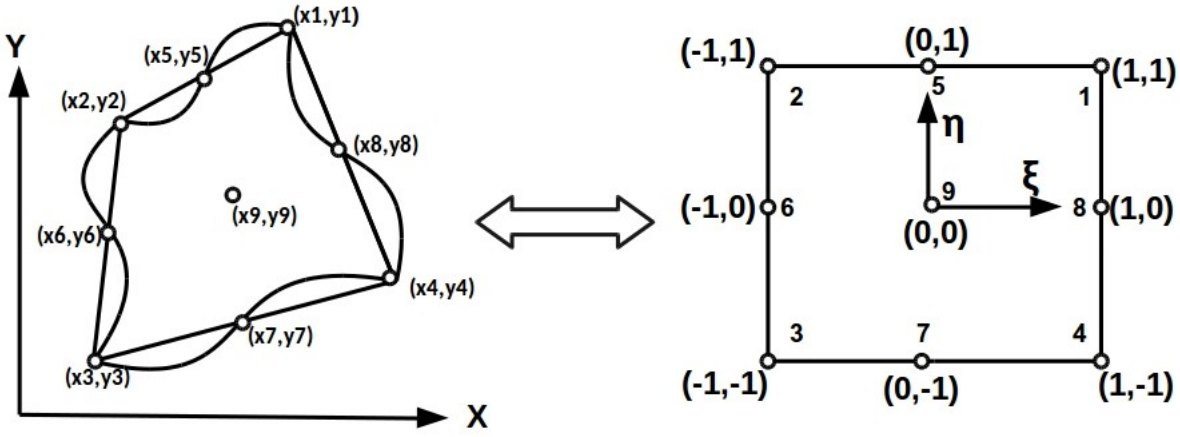

Figure 2.2: Transformation of 2D quadratic element to square cell

$$N(\xi_i,\eta_i) = \prod_{\substack{j=1 \\ i\neq j}}^{n} \prod_{\substack{k=1 \\ i\neq k}}^{n} \frac{(\xi-\xi_j).(\xi-\xi_{j+1})}{(\xi_i-\xi_j).(\xi_i-\xi_{j+1})} . \frac{(\eta-\eta_k).(\eta-\eta_{k+1})}{(\eta_i-\eta_k).(\eta_i-\eta_{k+1})} \tag{2.2}$$

here $(\xi_i,\eta_i) \subset \zeta$(local space) and n is number of nodes in a element. Using the above interpolation function, shape function (N_i) can be derived for each node. Similarly the above-mentioned transformation can be extended to a three dimensional element as shown in Fig. 2.3:

The iso-parametric transformation between the global and local domain for an element is shown in Eq. (2.3):

$$\begin{aligned} x &= \sum_{i=1}^{n} N_i.x_i = N_1x_1 + N_2x_2 + \cdots + N_nx_n \\ y &= \sum_{i=1}^{n} N_i.y_i = N_1y_1 + N_2y_2 + \cdots + N_ny_n \end{aligned} \tag{2.3}$$

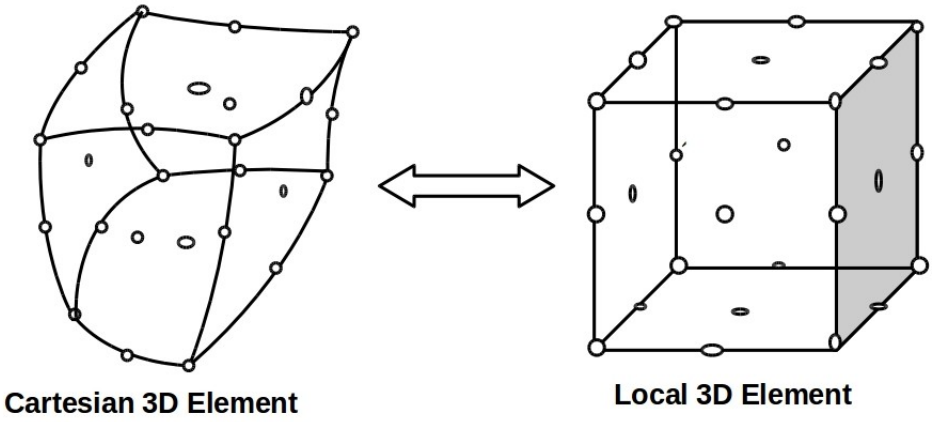

Figure 2.3: 3D transformation from $\hat{\zeta}(x,y,z)$ to $\zeta(\xi,\eta,\theta)$

here $(x_i, y_i) \subset \hat{\zeta}$ are the coordinates of i^{th} node. Final set of transformed equations in terms of coefficients is given as in Eq. (2.4)

$$\begin{aligned} x &= C_1\xi + C_2\eta + C_3\xi^2 + C_4\eta^2 + C_5\xi\eta + C_6\xi^2\eta + C_7\xi\eta^2 + C_8\xi^2\eta^2 \\ y &= D_1\xi + D_2\eta + D_3\xi^2 + D_4\eta^2 + D_5\xi\eta + D_6\xi^2\eta + D_7\xi\eta^2 + D_8\xi^2\eta^2 \end{aligned} \tag{2.4}$$

where C_i and D_i are coefficients in terms of x_i and y_i. The detailed expression of these coefficients are given in appendix-A. For a continuous function $\hat{f}(x,y) \in C^0(\hat{\zeta})$ in global space there $\exists$ a continuous function $f(\xi,\eta) \in C^0(\zeta)$ in local space as follows:

$$f(\xi,\eta) = \hat{f}(x(\xi,\eta), y(\xi,\eta)) \tag{2.5}$$

The corresponding inverse map of this one-one and onto mapping for a continuous function $\hat{f}$(x,y) is shown as:

$$\hat{f}(x,y) = f(\xi(x,y), \eta(x,y)) \tag{2.6}$$

For a second order differentiable function f, the first and second order derivatives of f with respect to x and y are obtained by the chain rule as:

$$\begin{cases} \hat{f}_x = f_\xi.\xi_x + f_\eta.\eta_x \\ \hat{f}_y = f_\xi.\xi_y + f_\eta.\eta_y \end{cases} \tag{2.7}$$

$$\begin{cases} \hat{f}_{xx} = f_\xi.\xi_{xx} + f_\eta.\eta_{xx} + \xi_x(g_{\xi\xi}.\xi_x + g_{\xi\eta}.\eta_x) + \eta_x(f_{\eta\xi}.\xi_x + g_{\eta\eta}.\eta_x) \\ \hat{f}_{yy} = f_\xi.\xi_{yy} + f_\eta.\eta_{yy} + \xi_y(g_{\xi\xi}.\xi_y + g_{\xi\eta}.\eta_y) + \eta_y(f_{\eta\xi}.\xi_y + g_{\eta\eta}.\eta_y) \\ \hat{f}_{xy} = f_\xi.\xi_{xy} + f_\eta.\eta_{xy} + s_x(g_{\xi\xi}.\xi_y + g_{\xi\eta}.\eta_y) + \eta_x(f_{\eta\xi}.\xi_y + g_{\eta\eta}.\eta_y) \end{cases} \tag{2.8}$$

Transformed PDEs from global to local domain are obtained by utilizing Eq. (2.7,2.8). These transformed PDEs contains first and second order derivatives like ($\xi_x, \xi_y, \xi_{xx}, \xi_{yy}$ etc.) of local coordinate system (ξ, η). The expression for calculating these derivative terms is written as:

$$\mathbf{J}(x,y) = \begin{bmatrix} \xi_x & \xi_y \\ \eta_x & \eta_y \end{bmatrix} = \mathbf{M}^{-1} \tag{2.9}$$

and

$$\begin{bmatrix} \xi_{xx} & \xi_{yy} \\ \eta_{xx} & \eta_{yy} \end{bmatrix} = -2\mathbf{J}(x,y). \begin{bmatrix} C_{11} & C_{12} \\ C_{21} & C_{22} \end{bmatrix} \tag{2.10}$$

where matrix $\mathbf{C}=\begin{bmatrix} C_{11} & C_{12} \\ C_{21} & C_{22} \end{bmatrix}$ and $\mathbf{M}=\begin{bmatrix} M_{11} & M_{12} \\ M_{21} & M_{22} \end{bmatrix}$. The detailed derivation of these matrix $\mathbf{C}$ and $\mathbf{M}$ is given in apprendix-B. The coefficients of matrix $\mathbf{M}$ are defined as:

$$\begin{aligned} M_{11} &= C_1 + C_5\eta + 2C_3\xi + 2C_6\xi\eta + C_7\eta^2 + 2C_8\xi\eta^2 \\ M_{12} &= C_2 + C_5\xi + 2C_4 + C_6\xi^2 + 2C_7\xi\eta + 2C_8\xi^2\eta \\ M_{21} &= D_1 + D_5\eta + 2D_3\xi + 2D_6\xi\eta + D_7\eta^2 + 2D_8\xi\eta^2 \\ M_{22} &= D_2 + D_5\xi + 2D_4 + D_6\xi^2 + 2D_7\xi\eta + 2D_8\xi^2\eta \end{aligned}$$

The detailed derivation of the Eq. (2.9, 2.10) are given in appendix-A. It should be noted that the elements of Jacobian matrix $\mathbf{J}$ are non-linear function of local space (ξ, η) for quadratic cells. However, these elements are linear function of local space for linear quadrilateral cells [8]. Details of the algebraic transformation of a four noded linear element into a square element is given by Nezami et al. [8]. The transformation described in this section allows NIM to map non-linear quadrilateral elements at curved boundary with square computational domains. This results better approximation of underlying physics at the boundary surface in comparison to the application of linear quadrilateral elements as used by Nezami et al. [8]. Thus a novel scheme is developed in the following sections utilizing non-linear elements at curved surfaces and linear elements for interior of domain.

2.2 Discretization of Domain

In present scheme physical domain is discretized with linear as well as quadratic quadrilateral elements. The quadratic elements are chosen for analogous mapping of curved surfaces while linear elements are used for inner domain as shown in Fig. 2.4. It should be noted that quadratic elements with 9 nodes of Lagrange family are used for boundaries and 4 noded linear elements are used for interior of the domain. The application of linear elements for whole geometry does

not fit accurately specially at the curved boundaries. In previously reported work [8, 13] the curved surfaces are linearly approximated and enforcement of boundary conditions also done on the linearized surface. Since linearization of curved surface at the boundary does not reflect the true nature of the geometry. Thus the curved boundaries are discretized using quadratic quadrilateral elements which preserve the nature of the geometry in much accurate way.

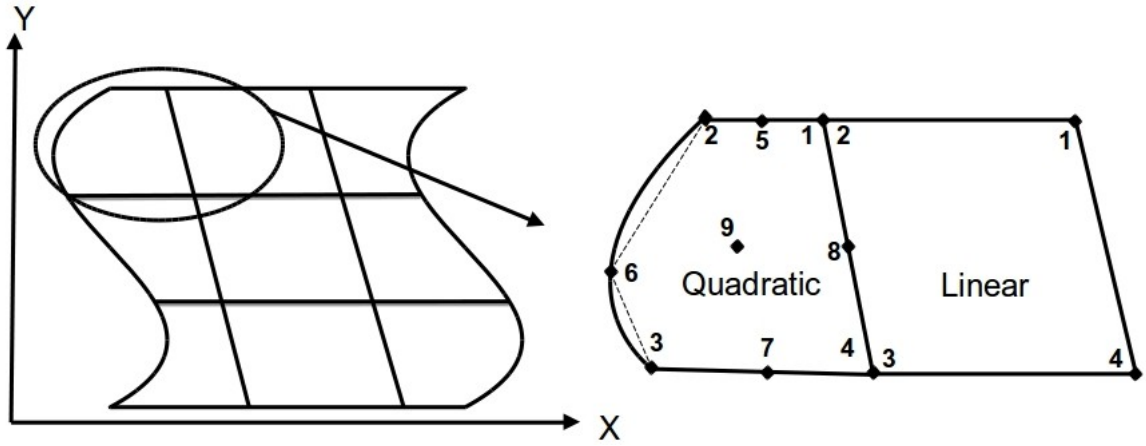

Figure 2.4: Discretization of arbitrary domain using linear and quadratic elements

The geometrical transformation of quadratic quadrilateral elements to square elements is described in previous section. Similarly the detailed description of the transformation of linear quadrilateral element with reference to NIM methodology is reported in Nezami et al. [8]. C^1 type continuity conditions are enforced at the interface of linear-linear and quadratic-linear elements. The complete discretization of problem domain using quadratic quadrilateral elements is unnecessary since the governing transport equations in fluid flow and heat transfer based on Eulerian frame of reference. In summary both linear as well as quadratic elements should be used for more accurate discretization.

2.3 Convection-Diffusion Equation As A Model Equation

The convection diffusion equation is chosen here as a model equation for detailed description of discretization procedure. The generalize form of two dimensional steady state advection diffusion equation in Cartesian coordinate system is:

$$u\frac{\partial \hat{T}}{\partial x} + v\frac{\partial \hat{T}}{\partial y} - \alpha\left(\frac{\partial^2 \hat{T}}{\partial x^2} + \frac{\partial^2 \hat{T}}{\partial x^2}\right) = \hat{f}(x,y) \tag{2.11}$$

where $\hat{f}(x,y)$ is the source function, α is thermal diffusivity and u, v are velocities in x and

y direction respectively. $\hat{T} \in \hat{\xi}$ is temperature distribution in global co-ordinate system. The transformed equation of Eq. (2.11) in local coordinate system using Eq. (2.7, 2.8) is given as:

$$\begin{aligned} \{(\xi_x u + \xi_y v) - \alpha(\xi_{xx} + \xi_{yy})\}\frac{\partial T}{\partial \xi} + \{(\eta_x u + \eta_y v) - \alpha(\eta_{xx} + \eta_{yy})\}\frac{\partial T}{\partial \eta} \\ -\{\alpha(\xi_{xx}^2 + \xi_{yy}^2)\frac{\partial^2 T}{\partial \xi^2} + \alpha(\eta_{xx}^2 + \eta_{yy}^2)\frac{\partial^2 T}{\partial \eta^2}\} - 2\alpha(\xi_x\eta_x + \xi_y\eta_y)\frac{\partial^2 T}{\partial \xi \partial \eta} = f(\xi, \eta) \end{aligned} \tag{2.12}$$

Above-mentioned transformed equation is further simplified as follows using the redefinition of terms.

$$u_c\frac{\partial T}{\partial \xi} + v_c\frac{\partial T}{\partial \eta} - (\alpha_\xi\frac{\partial^2 T}{\partial \xi^2} + \alpha_\eta\frac{\partial^2 T}{\partial \eta^2}) - 2\alpha(\xi_x\eta_x + \xi_y\eta_y)\frac{\partial^2 T}{\partial \xi \partial \eta} = f(\xi, \eta) \tag{2.13}$$

where

$$\begin{cases} u_c = \{(\xi_x u + \xi_y v) - \alpha(\xi_{xx} + \xi_{yy})\} \\ v_c = \{(\eta_x u + \eta_y v) - \alpha(\eta_{xx} + \eta_{yy})\} \\ \alpha_\xi = \alpha(\xi_{xx}^2 + \xi_{yy}^2) \\ \alpha_\eta = \alpha(\eta_{xx}^2 + \eta_{yy}^2) \end{cases}$$

In above transformed equation the redefined terms like (u_c, α_ξ etc) depend upon the velocity field, thermo physical properties as well as derivative of local coordinates (ξ_x, ξ_{xx} etc). These derivative terms depend on the type of transformation used for specific element. For quadratic elements, transformation Jacobians are non-linear and for linear elements Jacobians are linear in nature. Thus the redefined terms also depends upon the type of transformation utilized (quadratic or linear elements) for a particular discrete element.

2.3.1 Transverse Integration Procedure

The unique procedure of nodal integral method, TIP (Transverse Integration Procedure) is applied over transformed Eq. (2.13). This TIP is applied on the computational domain (ξ, η) using the transverse averaging operators $(1/2)\int_{-1}^{1} d\eta$ and $(1/2)\int_{-1}^{1} d\xi$. These averaging operators generate two transverse averaged ordinary differential equations in ξ and η directions respectively.

$$\bar{u}_c\frac{d\bar{T}^\eta}{d\xi} - \bar{\alpha}_\xi\frac{d^2\bar{T}^\eta}{d\xi^2} = \bar{S}_{1,0}^\eta \tag{2.14}$$

$$\bar{v}_c\frac{d\bar{T}^\xi}{d\eta} - \bar{\alpha}_\eta\frac{d^2\bar{T}^\xi}{d\eta^2} = \bar{S}_{2,0}^\xi \tag{2.15}$$

$\bar{S}^{\eta}_{1,0}$ and $\bar{S}^{\xi}_{2,0}$ are pseudo source terms. These pseudo source terms can be approximated by expanding them in Legendre polynomial and truncated them in lower orders. These kind of approximations are routinely used in NIM [2, 17, 22]. For $zero^{th}$ order truncation both pseudo source terms become constant which result into the second order approximation of scheme for regular Cartesian domains [2, 7, 17, 22, 23]. But this order may not be guaranteed in discretization of domain using non-orthogonal quadrilateral elements. In present scheme the pseudo source terms are truncated to $zero^{th}$ order. Each homogeneous term of Eq. (2.14 and 2.15) is obtained by the approximation, which says that average of products is approximated to the product of averages as shown in Eq. (2.16).

$$\frac{1}{2}\int_{-1}^{1} u_c \frac{\partial T}{\partial \xi} d\xi \approx \frac{1}{2}\int_{-1}^{1} u_c d\xi . \frac{1}{2}\int_{-1}^{1} \frac{\partial T}{\partial \xi} d\xi \tag{2.16}$$

The evaluation of terms $\bar{u}_c, \bar{\alpha}_{\xi}$ in Eq. (2.14) are approximated as below:

$$\bar{u_c} = \frac{1}{2}\int_{-1}^{1} u_c d\xi \approx \frac{1}{4}\int_{-1}^{1}\int_{-1}^{1} u_c d\xi d\eta = \frac{1}{4}\int_{-1}^{1}\int_{-1}^{1} \{(\xi_x u + \xi_y v) - \alpha(\xi_{xx} + \xi_{yy})\} d\xi d\eta \tag{2.17}$$

$$\bar{\alpha}_{\xi} = \frac{1}{2}\alpha\int_{-1}^{1} (\xi_{xx}^2 + \eta_{xx}^2) d\xi \approx \frac{1}{4}\alpha\int_{-1}^{1}\int_{-1}^{1} (\xi_{xx}^2 + \eta_{xx}^2) d\xi d\eta \tag{2.18}$$

The right hand sides of Eq. (2.17 and 2.18) are evaluated for linear elements by treating each cell averaged terms separately as given in Eq. (2.19) [8, 12].

$$\begin{aligned} \overline{(\xi_x u + \xi_y v) - \alpha(\xi_{xx} + \xi_{yy})} &= \overline{\xi_x}.u + \overline{\xi_y}.v - \overline{\alpha\xi_{xx}} - \overline{\alpha\xi_{yy}} \\ \overline{\alpha(\xi_{xx}^2 + \xi_{yy}^2)} &= \overline{\alpha\xi_{xx}^2} + \overline{\alpha\xi_{yy}^2} \end{aligned} \tag{2.19}$$

For linear elements the Jacobians are linear in nature and thus individual treatment of terms doesn't affect the cell averaging procedure. While the transformation Jacobians are higher order in case of quadratic elements as described in previous section. These higher order Jacobians contains more feature of curved geometries. Thus for quadratic elements these approximations are obtained by cell averaging the whole term instead of individual in the following manner (Eq. (2.20)).

$$\begin{aligned} \overline{(\xi_x u + \xi_y v) - \alpha(\xi_{xx} + \xi_{yy})} &= \overline{\xi_x.u + \xi_y.v} - \overline{\alpha(\xi_{xx} - \xi_{yy})} \\ \overline{\alpha(\xi_{xx}^2 + \xi_{yy}^2)} &= \overline{\alpha(\xi_{xx}^2 + \xi_{yy}^2)} \end{aligned} \tag{2.20}$$

This modification improves the accuracy of overall scheme for quadratic quadrilateral elements. The pseudo source terms of the transverse average ODEs generated after TIP procedure

are also cell averaged in the following way.

$$\begin{aligned} \int_{-1}^{1} \bar{S}^{\eta}_{1,0}(\xi)d\xi &\approx \bar{S}^{\eta\xi}_{1,0} \\ \int_{-1}^{1} \bar{S}^{\xi}_{2,0}(\eta)d\eta &\approx \bar{S}^{\xi\eta}_{2,0} \end{aligned} \tag{2.21}$$

The cell averaged equations (Eq. (2.14 and 2.15)), obtained after TIP procedure, are coupled to each other, but the truncation of each pseudo-source terms decouples these equations [7]. The cell analytical solutions, generated from the ODEs (Eq. (2.14 and 2.15)), contain geometric transformation as well as nature of underlying physics (Advection and Diffusion). The cell analytical solution for Eq. (2.14) is given as:

If $\bar{u}_c = 0$

$$\bar{T}^{\eta}(\xi) = \frac{\bar{S}^{\eta\xi}_{1,0(i,j)}}{2\bar{\alpha}_{\xi(i,j)}}\xi^2 + K_1\xi - K_2 \tag{2.22}$$

If $\bar{u}_c \neq 0$

$$\bar{T}^{\eta}(\xi) = K_3.e^{\left\{\frac{\bar{u}_{c(i,j)}}{\bar{\alpha}_{\xi(i,j)}}\xi\right\}} + \frac{\bar{S}^{\eta\xi}_{1,0(i,j)}}{\bar{u}_{c(i,j)}}\xi + K_4 \tag{2.23}$$

where integral constants K_i are calculated by applying boundary values of $\bar{T}^{\eta}(\xi)$ for each cell as shown in Figure 2.5. Since $\bar{T}^{\eta}_{\xi}$ is the transverse averaged temperature rather than point values thus the discrete numerical solution obtained by NIM methodology are in terms of surface averaged values. Hence the temperature of each cell surface is unique.

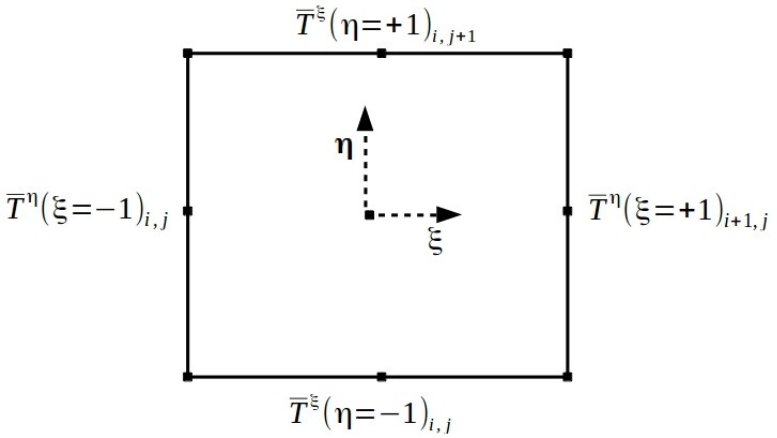

Figure 2.5: Value of transverse averaged variable $\bar{T}$ at cell boundaries

In Eq. (2.23) exponential term drives the transport phenomenon of advection-diffusion equation over each cell and leads to inherent upwinding. These transcendental cell analytical solutions are the interpolation functions of the field variables in discrete space and inherit the nature

of the physics since they are generated from the governing differential equations of the physics. Thus the interpolation of dependent variable leads to much accurate NIM scheme with coarser grids in comparison to other contemporary numerical methods. It also allows to calculate the values of dependent variables at any point inside a cell using cell analytical solutions. Similarly the cell analytical solution for η direction $\bar{T}^{\xi}(\eta)$ can be obtained for $(i,j)^{th}$ cell on solving the Eq. (2.15).

2.3.2 Continuity and Constrain conditions

As discussed in the previous section the cell analytical solutions are valid over individual cells hence the coupling of these solutions between the two neighboring cells are enforced by application of continuity conditions at the interface of cells. The enforced continuity conditions between the cells are C^1 type (Eq. (2.24)).

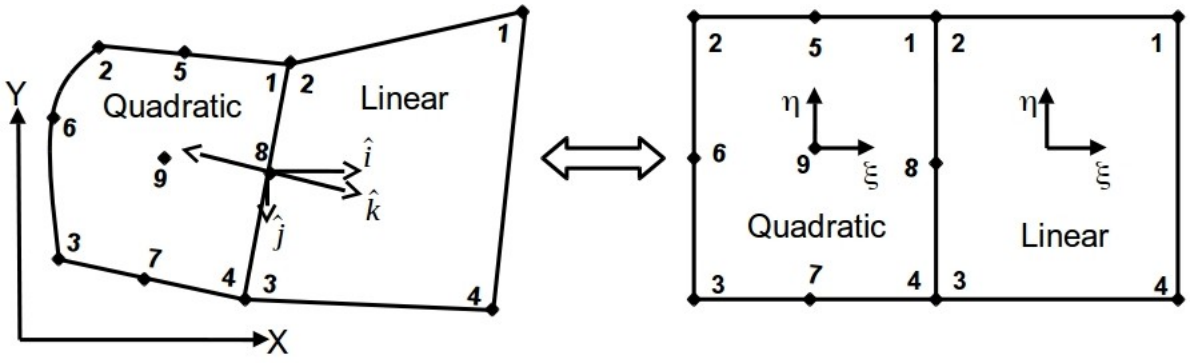

Figure 2.6: Discretization of arbitrary domain using linear and quadratic elements

For non-orthogonal grids, the orientation of the interface will also involved in enforcement of continuity conditions. Figure 2.6 represents the application of continuity conditions between quadratic and linear cells where $\hat{k}$ represents the normal unit vector at interface and $\hat{i},\hat{j}$ are the unit vectors in x and y direction respectively. However these type of continuity conditions are also valid between the adjacent linear elements. The first continuity condition is relatively straightforward; the continuity of dependent variable. However, the second continuity condition is the continuity of derivatives at the interface of adjacent cells, either linear-linear or quadratic-linear, as given in Eq. (2.24) .

$$\begin{aligned} \hat{T}^{\eta}_{i,j}\Big|_{14} &= \hat{T}^{\eta}_{i+1,j}\Big|_{23} = \hat{T}_{i,j} \\ \frac{d\hat{T}_{i,j}}{dk}\Big|_{14} &= \frac{d\hat{T}_{i,j}}{dk}\Big|_{23} \end{aligned} \tag{2.24}$$

For application of the second continuity condition, the derivatives of dependent variables with respect to global co-ordinates (x,y) are transformed to local co-ordinates(ξ,η) using equation Eq. (2.7) as follows:

$$\frac{d\hat{T}_{i,j}}{dk} = \frac{d\hat{T}_{i,j}}{dx}m_x + \frac{d\hat{T}_{i,j}}{dy}m_y \tag{2.25}$$

where m_x and m_y are the direction cosines of cell surface in x and y direction respectively. The corresponding transformed equation of Eq. (2.25) is:

$$\frac{d\hat{T}_{i,j}}{dk} = \{T_\xi \xi_x + T_\eta \eta_x\}m_x + \{T_\xi \xi_y + T_\eta \eta_y\}m_y \tag{2.26}$$

In Eq. (2.26) the derivatives of local dependent variable T are approximated in the following manner:

$$\frac{d\hat{T}_{i,j}}{dk} = \left\{\frac{\partial \hat{T}^\eta}{\partial \xi}\xi_x + \frac{T_{p(i,j+1)} - T_{p(i,j)}}{2\Delta\eta}\eta_x\right\}m_x + \left\{\frac{\partial \hat{T}^\eta}{\partial \xi}\xi_y + \frac{T_{p(i,j+1)} - T_{p(i,j)}}{2\Delta\eta}\eta_y\right\}m_y \tag{2.27}$$

where the derivative $(\partial\hat{T}/\partial\xi)$ are evaluated by differentiating the cell analytical solutions (Eq. (2.22 and 2.23)). $T_{p(i,j)}$ are point values and evaluated by the linear approximation of connected cells at a common vertexes. The final form of second continuity condition is obtained

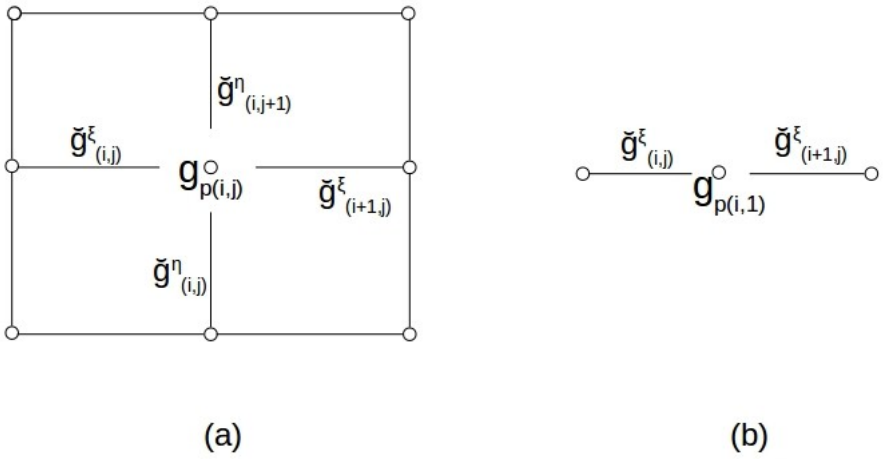

Figure 2.7: Calculation of point values of temperature T_p

by using Eqs. (2.24 and 2.25) for two adjacent cells $(i,j)^{th}$ and $(i+1,j)^{th}$.

$$\left\{(m_x\xi_x + m_y\xi_y)_{(i,j)}\frac{\partial \hat{T}^\eta_{i,j}}{\partial\xi}\bigg|_{\xi=+1}\right\} + \left\{(m_x\eta_x + m_y\eta_y)_{(i,j)}\left(\frac{T_{p(i,j+1)} - T_{p(i,j)}}{2\Delta\eta}\right)\right\} \tag{2.28}$$

$$= \left\{(m_x\xi_x + m_y\xi_y)_{(i+1,j)}\frac{\partial \hat{T}^\eta_{i+1,j}}{\partial\xi}\bigg|_{\xi=-1}\right\} + \left\{(m_x\eta_x + m_y\eta_y)_{(i+1,j)}\left(\frac{T_{p(i,j+1)} - T_{p(i,j)}}{2\Delta\eta}\right)\right\}$$

Using both the continuity conditions between the two neighboring cells (Fig. (2.6)) leads to a three point scheme as given in Eq.(2.29, 2.30) for ξ and η direction respectively.

$$\begin{aligned} &A_1.\bar{T}^{\eta}_{(i-1,j)} - (A_1+A_2).\bar{T}^{\eta}_{(i,j)} + A_2.\bar{T}^{\eta}_{(i+1,j)} = A_3.\bar{S}^{\eta\xi}_{1(i,j)} + A_4.\bar{S}^{\eta\xi}_{1(i+1,j)} \\ &-\left(\frac{T_{p(i,j+1)} - T_{p(i,j)}}{2}\right)\Big\{(m_x\eta_x + m_y\eta_y)_{i+1,j} - (m_x\eta_x + m_y\eta_y)_{i,j}\Big\} \end{aligned} \tag{2.29}$$

$$\begin{aligned} &B_1.\bar{T}^{\xi}_{(i,j-1)} - (B_1+B_2).\bar{T}^{\xi}_{(i,j)} + B_2.\bar{T}^{\xi}_{(i,j+1)} = B_3.\bar{S}^{\xi\eta}_{2(i,j)} + B_4.\bar{S}^{\xi\eta}_{2(i,j+1)} \\ &-\left(\frac{T_{p(i+1,j)} - T_{p(i,j)}}{2}\right)\Big\{(m_x\xi_x + m_y\xi_y)_{i,j+1} - (m_x\xi_x + m_y\xi_y)_{i,j}\Big\} \end{aligned} \tag{2.30}$$

where A_i and B_i are coefficients of three point schemes. The expanded form of these terms are given in appendix B. These three point schemes contain pseudo source terms $\bar{S}_1$ and $\bar{S}_2$. Thus two more equations are required for closure. These extra equations are generated by application of physically relevant constraint conditions [3, 12]. In the first constraint condition cell averaging operator $\frac{1}{4}\int_{-1}^{1}\int_{-1}^{1} d\xi d\eta$ is applied over the transformed PDE Eq. (2.13). This results a relation between pseudo source terms and actual source term as shown in Eq. (2.31).

$$\bar{S}^{\eta\xi}_{1(i,j)} + \bar{S}^{\xi\eta}_{2(i,j)} = \bar{f}^{\eta\xi} - \frac{1}{4}\int_{-1}^{+1}\int_{-1}^{+1} 2\alpha(\xi_x\eta_x + \xi_y\eta_y)T_{\xi\eta}d\xi d\eta \tag{2.31}$$

Again the right hand side terms of Eq. (2.31) are approximated in a similar way as described in Eq. (2.20). The second constraint condition is uniqueness of cell averaged values of dependent variables. Thus the cell averaged value is independent of the order of directional averaging i.e $\bar{T}^{\xi\eta}_{i,j} = \bar{T}^{\eta\xi}_{i,j}$. Final set of discrete equations are generated with the application of these two constraint conditions. The form of the set of final discrete equations (Eqs. (2.32 and 2.33)) is similar to the equations derived by Kumar et al. [11] for linear quadrilateral elements.

$$\begin{aligned} &F_{11}\bar{T}^{\xi}_{i,j-1} - F_{12}\bar{T}^{\xi}_{i,j} + F_{13}\bar{T}^{\xi}_{i,j+1} + F_{14}\bar{T}^{\eta}_{i-1,j} + F_{15}\bar{T}^{\eta}_{i,j} - F_{16}\bar{T}^{\eta}_{i-1,j+1} - F_{17}\bar{T}^{\eta}_{i,j+1} \\ &= F_{18}f_{1(i,j)} - F_{19}f_{1(i,j+1)} - \left(\frac{T_{p(i+1,j)} - T_{p(i,j)}}{2}\right)\Big\{(m_x\xi_x + m_y\xi_y)_{i+1,j} - (m_x\xi_x + m_y\xi_y)_{i,j}\Big\} \end{aligned} \tag{2.32}$$

$$\begin{aligned} &F_{21}\bar{T}^{\eta}_{i-1,j} - F_{22}\bar{T}^{\eta}_{i,j} + F_{23}\bar{T}^{\eta}_{i+1,j} + F_{24}\bar{T}^{\xi}_{i,j-1} + F_{25}\bar{T}^{\xi}_{i,j} - F_{26}\bar{T}^{\xi}_{i+1,j-1} - F_{27}\bar{T}^{\xi}_{i+1,j} \\ &= F_{28}f_{1(i,j)} - F_{29}f_{1(i+1,j)} - \left(\frac{T_{p(i,j+1)} - T_{p(i,j)}}{2}\right)\Big\{(m_x\eta_x + m_y\eta_y)_{i+1,j} - (m_x\eta_x + m_y\eta_y)_{i,j}\Big\} \end{aligned} \tag{2.33}$$

where F_{ij} are the coefficients of final discrete equations. The detailed expression of these coefficients are give in appendix-B.

2.4 Diffusion Equation

The general form of two dimensional Poisson equation or 2D steady state diffusion equation in Cartesian coordinate system, is given by:

$$\nabla^2 \hat{T} = \hat{f}(x,y) \tag{2.34}$$

and the corresponding transformed equation in (ξ, η) local coordinate system is:

$$\begin{aligned}(\xi_{xx}+\xi_{yy})T_\xi + (\eta_{xx}+\eta_{yy})T_\eta + (\xi_{xx}^2+\xi_{yy}^2)T_{\xi\xi} + (\eta_{xx}^2+\eta_{yy}^2)T_{\eta\eta} \\ +2(\xi_x\eta_x+\xi_y\eta_y)T_{\xi\eta} = f(\xi,\eta)\end{aligned} \tag{2.35}$$

Since the transformed diffusion equation is similar to the transformed advection-diffusion equation except the velocity terms appearing in Eq. (2.12). Thus further procedure of discretization of transformed diffusion equation (Eq. (2.35) by NIM is similar to the scheme developed for advection-diffusion equation. The detailed development of the scheme for diffusion equations is not shown here for the sake of brevity.

2.5 Non-linear Equations (Navier-Stokes)

Again scheme for Navier-Stokes equations is developed with reference to the scheme developed for the convection diffusion equation as discussed in previous section. The primitive form of two dimensional steady state Navier-Stokes equations in global coordinate system is:

$$\frac{\partial \hat{u}}{\partial x} + \frac{\partial \hat{v}}{\partial y} = 0 \tag{2.36}$$

$$\hat{u}\frac{\partial \hat{u}}{\partial x} + \hat{v}\frac{\partial \hat{u}}{\partial y} - \nu\left\{\frac{\partial^2 \hat{u}}{\partial x^2} + \frac{\partial^2 \hat{u}}{\partial y^2}\right\} - \frac{1}{\rho}\frac{\partial \hat{p}}{\partial x} + \hat{b}_x = 0 \tag{2.37}$$

$$\hat{u}\frac{\partial \hat{v}}{\partial x} + \hat{v}\frac{\partial \hat{v}}{\partial y} - \nu\left\{\frac{\partial^2 \hat{v}}{\partial x^2} + \frac{\partial^2 \hat{v}}{\partial y^2}\right\} - \frac{1}{\rho}\frac{\partial \hat{p}}{\partial y} + \hat{b}_y = 0 \tag{2.38}$$

where x, y are the independent spatial variables and $\hat{b}_x, \hat{b}_y$ are the body force term in x and y direction respectively. The $\hat{u}$, $\hat{v}$ and $\hat{p}$ are velocity components and pressure in global domain. The continuity condition is oftenly replaced by the elliptic form of pressure Poisson equation. The pressure Poisson equation in terms of pressure correction p' is:

$$\frac{\partial^2 p'}{\partial x^2} + \frac{\partial^2 p'}{\partial y^2} = \left[\frac{\partial u^*}{\partial x} + \frac{\partial v^*}{\partial y}\right] \tag{2.39}$$

Eqs. (2.37 and 2.38) along with Eq. (2.39) are mathematically similar to the set of Eqs. (2.36, 2.37 and 2.38). Since N-S equations are non-linear in nature the convective terms of the equa-

tions are approximated to generate cell analytical solution. These approximations are introduced by taking the cell averaged velocity in convection terms of the N-S equations which are defined as:

$$\bar{u}_{c(i,j)} = \frac{\bar{u}^{\eta}_{i,j} + \bar{u}^{\eta}_{i+1,j} + \bar{u}^{\xi}_{i,j} + \bar{u}^{\xi}_{i,j+1}}{4} \tag{2.40}$$

$$\bar{v}_{c(i,j)} = \frac{\bar{v}^{\eta}_{i,j} + \bar{v}^{\eta}_{i+1,j} + \bar{v}^{\xi}_{i,j} + \bar{v}^{\xi}_{i,j+1}}{4} \tag{2.41}$$

With reference to the Figure 2.5, the cell average velocities for $(i,j)^{th}$ cell are evaluated by taking the mean of cell surface velocities (Eq. (2.40)). These approximations are verified and tested in the previously developed schemes for N-S equations by Kai et al. [24] and Kumar et al. [13]. This leads, linear form of governing N-S equations similar to the convection diffusion equation.

$$V\nabla V \approx V_c \nabla V \tag{2.42}$$

The only difference is the source term which is pressure gradient as well as body force terms. Along with the momentum equations, pressure Poisson equation is solved to obtained the divergence free velocity field. Here the pressure Poisson equation is similar to the equation used in SIMPLE algorithm. The pressure and velocity coupling is obtained by utilizing the pressure correction algorithm proposed by Kumar et al. [11] with reference to the NIM methodology.

2.6 Boundary Conditions Enforcement for Quadratic elements

In the present scheme the implementation of boundary conditions over a curved surface is done by piecewise linear approximation of a curved boundary. Dirichlet and Neumann type boundary conditions for linear quadrilateral elements for NIM methodology has been developed by Kumar et al. [13]. For quadratic elements Dirichlet boundary condition is straightforward. However the implementation of Neumann boundary condition is not trivial on curvature boundary. Thus piecewise linearization is done for quadratic elements on the curved surface as shown in the Fig. 2.8. The Neumann boundary condition is applied on each linear segment of quadratic element. Same cell analytical solution for a quadratic cell is utilized to enforce Neumann boundary condition over the two different linearized surface of quadratic element.

$$\frac{\partial \hat{\phi}}{\partial k} = \frac{\partial \hat{\phi}}{\partial x} m_x + \frac{\partial \hat{\phi}}{\partial y} m_y \tag{2.43}$$

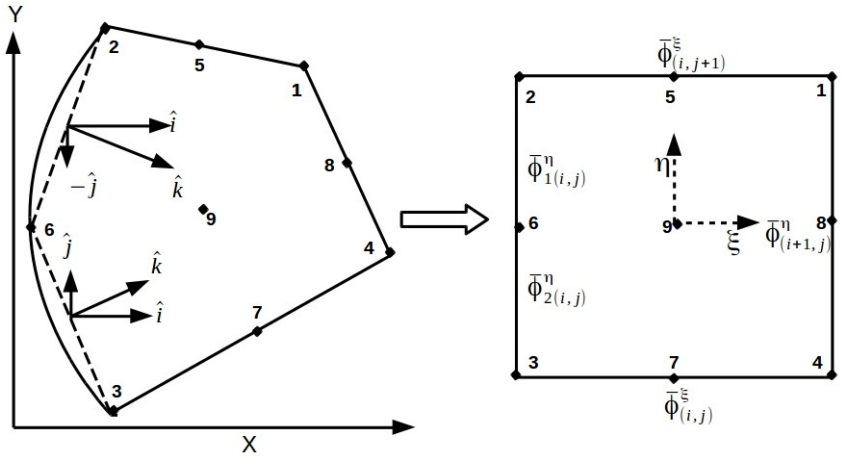

Figure 2.8: Piecewise linearization of curved surface of a quadratic elements

General form of Neumann boundary condition at a surface can be written as in Eq. (2.43) where m_x and m_y are direction cosines in x and y direction respectively and $\hat{k}$ is normal unit vector as used in continuity condition. Now on a quadratic edge (2-3), gradient is calculated over two piecewise linearized surfaces (2-6) and (6-3) as follows:

$$\left.\frac{\partial\hat{\phi}}{\partial k}\right|_{2-6} = \left(\frac{\partial\hat{\phi}}{\partial x}m_x\right)_{2-6} + \left(\frac{\partial\hat{\phi}}{\partial y}m_y\right)_{2-6} \tag{2.44}$$

$$\left.\frac{\partial\hat{\phi}}{\partial k}\right|_{6-3} = \left(\frac{\partial\hat{\phi}}{\partial x}m_x\right)_{6-3} + \left(\frac{\partial\hat{\phi}}{\partial y}m_y\right)_{6-3} \tag{2.45}$$

The Eq. (2.44 and 2.45) are transformed into the computational domain (ξ,η) for both the surfaces and the corresponding transformed equations are given as Eq. (2.46, and 2.47):

$$\left.\frac{\partial\hat{\phi}}{\partial k}\right|_{2-6} = \left(\frac{\partial\bar{\phi}^{\eta}}{\partial\xi}\xi_x + \frac{\partial\bar{\phi}^{\eta}}{\partial\eta}\eta_x\right)m_x\Bigg|_{2-6} + \left(\frac{\partial\bar{\phi}^{\eta}}{\partial\xi}\xi_y + \frac{\partial\bar{\phi}^{\eta}}{\partial\eta}\eta_y\right)m_y\Bigg|_{2-6} \tag{2.46}$$

$$\left.\frac{\partial\hat{\phi}}{\partial k}\right|_{6-3} = \left(\frac{\partial\bar{\phi}^{\eta}}{\partial\xi}\xi_x + \frac{\partial\bar{\phi}^{\eta}}{\partial\eta}\eta_x\right)m_x\Bigg|_{6-3} + \left(\frac{\partial\bar{\phi}^{\eta}}{\partial\xi}\xi_y + \frac{\partial\bar{\phi}^{\eta}}{\partial\eta}\eta_y\right)m_y\Bigg|_{6-3} \tag{2.47}$$

In the above equations gradient of dependent variable in ξ direction is obtained from the cell analytical solution $\bar{\phi}^{\eta}(\xi)$. However the gradient in η direction is calculated by utilizing the discrete value of the field variable calculated at each node of the cell. Since in NIM methodology the values are available at cell surfaces in terms of transverse averaged values as shown in Fig. 2.8. The point values at the node points of quadrilateral element are calculated by averaging the nearest cell surfaces values available to a corresponding point. The details of the evaluation of discrete point values is given by Kumar et al.[13]. Thus in Eq. (2.46 and 2.47)

the gradients of dependent variable in η direction are evaluated as given in Eq. (2.48 and 2.49)

$$\frac{\partial \bar{\phi}}{\partial \eta}\Big|_{2-6} = \frac{\phi_2 - \phi_6}{d\eta/2} \tag{2.48}$$

$$\frac{\partial \bar{\phi}}{\partial \eta}\Big|_{6-3} = \frac{\phi_6 - \phi_3}{d\eta/2} \tag{2.49}$$

The expression of Neumann boundary condition at each linearized surface contains point value of dependent variable ϕ_6 which is further approximated in terms of connected surface values of field variable $(\bar{\phi}^{\eta})_{2-6}$ and $(\bar{\phi}^{\eta})_{6-3}$ as:

$$\phi_6 = \frac{\bar{\phi}^{\eta}_{2-6} + \bar{\phi}^{\eta}_{6-3}}{2} \tag{2.50}$$

This leads to the close form implementation of the Neumann boundary condition on the curved surface utilizing quadratic quadrilateral elements. Similarly we can enforce mixed type boundary conditions on quadratic surfaces by careful application of above approximations.

Chapter 3

Numerical Results and Discussion

The schemes based on Nodal Integral Method using non-linear and linear quadrilateral elements has been tested for both linear and non-linear governing differential equations. The diffusion and convection-diffusion equations are solved in 2D cylindrical wedge domain and the results are compared with the analytical solutions. Both Neumann and Dirichlet type of boundary conditions are applied and tested in these cases. In all the cases, quadratic quadrilateral

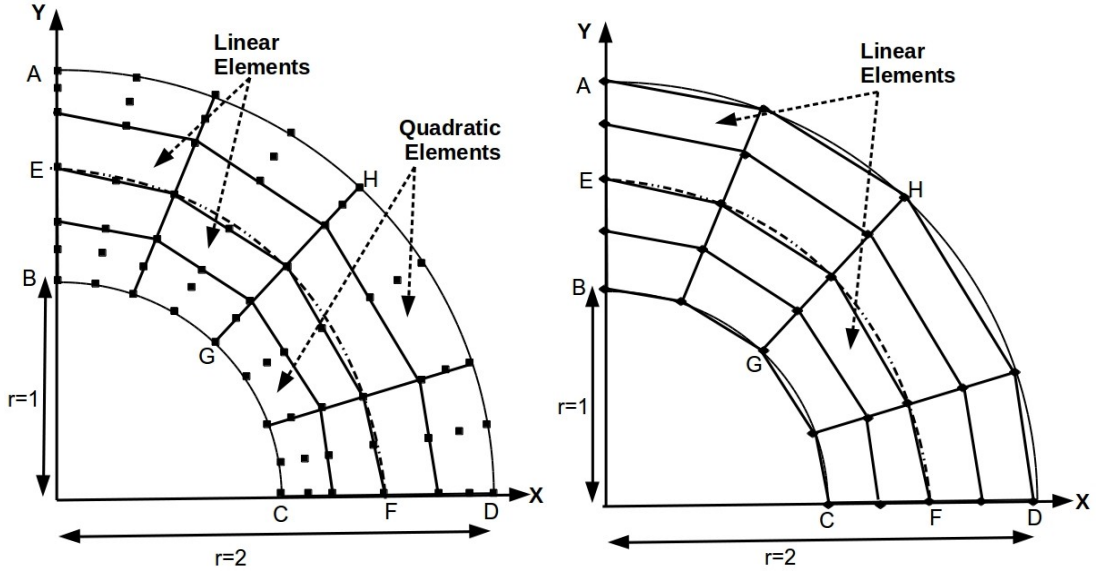

(a) (b)

Figure 3.1: Different discretization scheme used in NIM (a) Scheme-1 (b) Scheme-2

elements are applied to map the curvature boundary of the physical domain and internal nodal cells are linear quadrilateral elements as shown in Figure 3.1(a). The above mentioned scheme is also compared with the scheme based on complete linear discretization of whole domain as shown in Figure 3.1(b). Thus here onwards we will refer discretization using quadratic-linear quadrilateral elements as scheme-1 (Figure 3.1(a)) and discretization of whole domain using linear quadrilateral elements as scheme-2 (Figure 3.1(b)). The comparative studies have been done between the results obtained from both type of discretization procedure. Numerical scheme, based on the discretization procedure of scheme-1, is further applied to solve the

Navier-Stokes equations in 2D cylindrical wedge domain. Polar lid driven cavity is chosen as a test problem for validation of the numerical results with previously reported numerical and experimental results by Fuchs et al. [1].

3.1 Diffusion Equation

3.1.1 Neumann Boundary Condition

In this test case Laplace equation $\nabla^2 T = 0$ is numerically solved over a 2D cylindrical wedge domain with wedge boundaries $1 \leq r \leq 2$; $0 \leq \theta \leq \pi/2$ as shown in the Figure 3.1. The boundary conditions are Dirichlet type at surface AB, CD and AD ($T_{(r,\pi/2)} = T_{(r,0)} = 1$ and $T_{(2,\theta)} = 0$ respectively) and one Neumann condition $dT/dr|_{(1,\theta)} = 0$ on BC side of the wedge. The applicability of this numerical scheme for Neumann boundary condition is tested in this test problem. Numerical results are compared with analytical solution. The scheme based on Nodal integral methods have ability to produce reasonably accurate results on very coarse grid structure [2, 6, 7, 15].

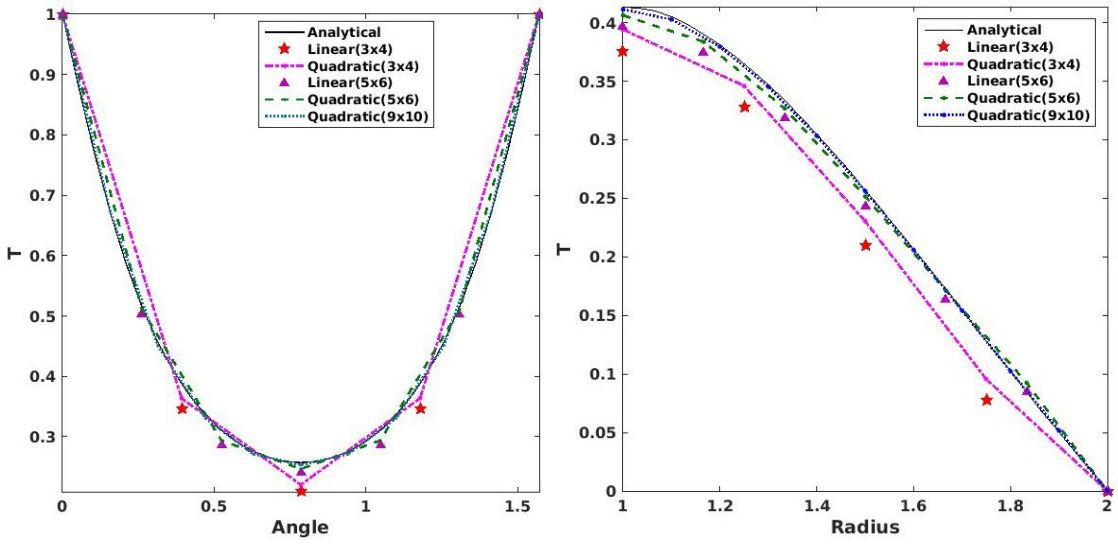

(a) (b)

Figure 3.2: Variation of temperature (a)Along EF at r=1.5 and $0 \leq \theta \leq \pi/2$ (b) Along GH at $\theta = \pi/4$ and $1 \leq r \leq 2$

Thus very coarse grid structure are chosen to show its effectiveness for the comparative study. For qualitative comparison, results are compared at central lines EF and GH as shown in Figure 3.1. Computation is done with different type of grid sizes. Figure 3.2(a) and 3.2(b)

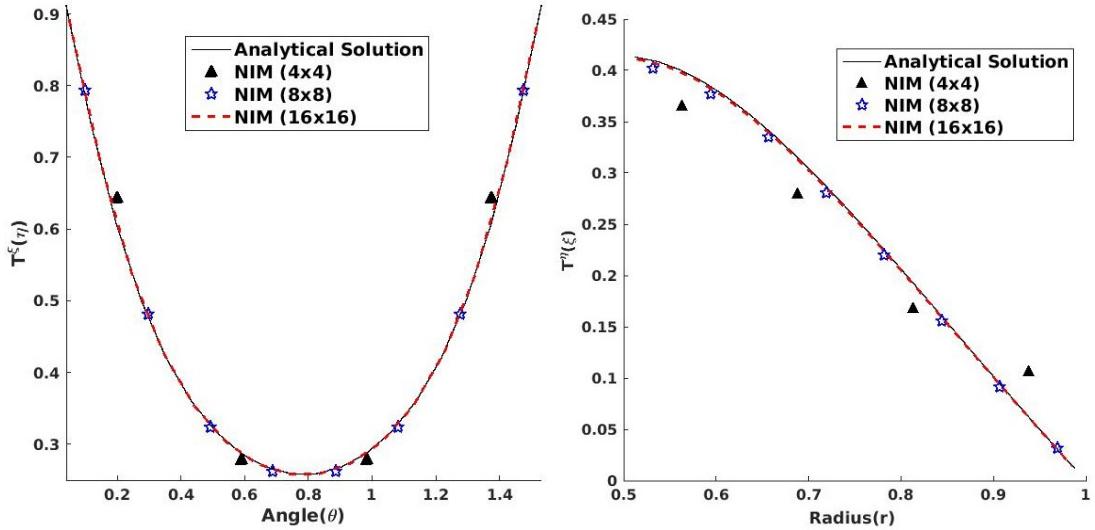

(a) (b)

Figure 3.3: Temperature distribution using scheme-1 (a)Along EF at r=1.5 and $0 \leq \theta \leq \pi/2$ (b) Along GH at $\theta = \pi/4$ and $1 \leq r \leq 2$

show the variation of temperature along the centerlines EF and GH respectively. The discrete temperatures along EF and GH generated by scheme-1 (quadratic-linear quadrilateral elements) as well as by scheme-2 (linear quadrilateral elements) using the mesh sizes (3×4), (5×6) and (9×10) are also shown in these plots. Both the schemes are compared with reference to analytical solutions.

It should be noted that the results obtained from the scheme-1 on similar mesh sizes are closer to analytical solution in comparison to scheme-2. It is concluded that effect of quadratic elements in scheme-1 is significant at very coarse grids (3×4). More realistic mapping of curvature boundaries utilizing the quadratic quadrilateral elements (scheme-1) enhance the accuracy of NIM in comparison to scheme-2. Further refinement of grid sizes monotonically reduces the deviation of the results in comparision to the analytical results. Results for grid sizes (9×10) using scheme-1 are also shown in Figure 3.2, which agree fairly well with analytical solutions. Effect of implementation of Neumann boundary condition is visible in these plots specifically along center line GH as shown in Figure 3.2(b). It should be noted that the boundary temperature at r=1 obtained by Neumann boundary condition (Figure 3.2(b)) is much closer for scheme-1 compared to scheme-2. Thus piecewise linearization of the curved surface using quadratic elements for Neumann boundary conditions plays an effective role in improvement of NIM methodology. Detailed quantitative comparison is also done to observe the behavior

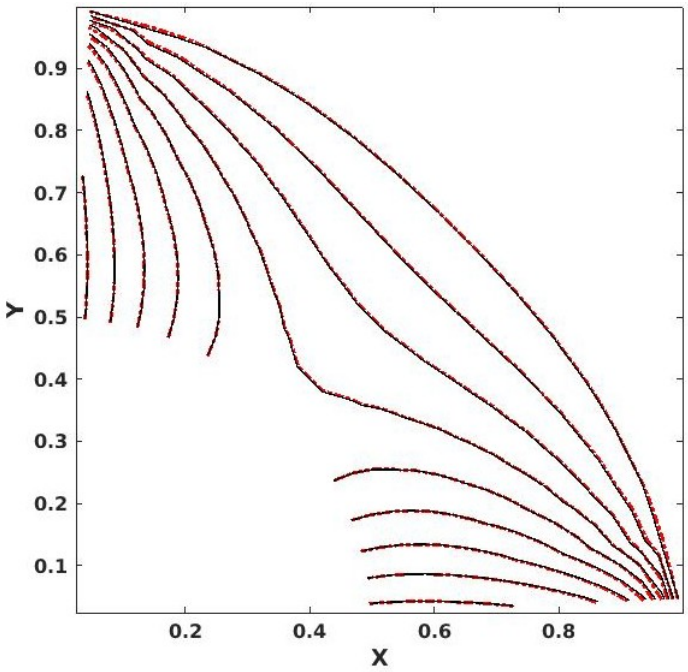

Figure 3.4: Temprature distribution over 2D cylinderical wedge domain for Neumann Bc

of numerical scheme toward quadratic elements. Table-3.1 contains L2 norm errors for whole

Table 3.1: L2 norm error for test case-1 for all grids and for boundary cells

Mesh	Total L2 norm error		Neumann boundary L2 norm error	
	Scheme-1	Scheme-2	Scheme-1	Scheme-2
4×4	1.2743×10^{-2}	1.4505×10^{-2}	5.5114×10^{-3}	1.4485×10^{-2}
8×8	3.3356×10^{-3}	3.5802×10^{-3}	1.6808×10^{-3}	4.1483×10^{-3}
16×16	8.8595×10^{-4}	9.1861×10^{-4}	4.6946×10^{-4}	1.1026×10^{-3}

domain as well as at the boundary surface where the Neumann boundary condition is applied (surface BC, Figure 3.1). Different grid sizes (4×4), (8×8) and (16×16) are used to calculate L2 norm errors for both the schemes.

From the table-3.1 it is noted that for coarsest grid (4×4) the numerical error for whole domain using scheme-1 is nearly 1.13 times more accurate than scheme-2. However at the Neumann boundary, scheme-1 is nearly 2.62 times more accurate than scheme-2. As the number of grids increases relative error between scheme-1 and scheme-2 reduces monotonically. This behavior of L2 norm error for boundary cells can be seen in Fig. 3.5 for different grid

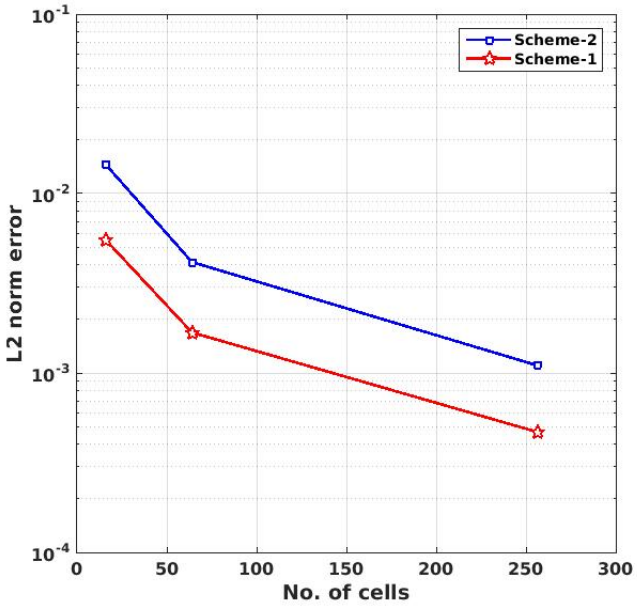

Figure 3.5: Variation of L2-norm error for test case-1 at Neumann boundary BC

sizes $(4\times4),(8\times8)$ and (16×16). It is observed from Fig. 3.5 that errors for scheme-1 are significantly less than scheme-2. Thus it is concluded from the above results that utilization of quadratic elements to map the curved surface improves the efficiency of NIM scheme.

3.1.2 Dirichlet Boundary Condition

Second test case is designed to test the scheme with Dirichlet boundary conditions. In this case Laplace equation in a square domain$(0\leq L1\leq 1)$,$(0\leq L2\leq 1)$ with fix boundary conditions $T(x,0)=T(L_1,y)=T(0,y)=0$ and $T(x,L_2)=1$; is opted, refer Fig. 3.6. In Fig. 3.6 Laplace equation is numerically solved in 2D cylindrical wedge domain ABCD with radius $1\leq r\leq 2$ and $0\leq\theta\leq\pi/2$.

Boundary condition of ABCD is given by analytical solution in a rectangular domain. Domain is discretized by body-fitted non-orthogonal quadratic elements with linear elements. A schematic representation of grids is given in Fig. 3.6. Previously reported limitation of curved boundary is much eased in present scheme[13]. Numerical solution is obtained for much coarser non-uniform grids (3x4), (5x6) with quadratic-linear discretization and compared with linear as well as analytical solution in Fig. 3.7. It is observed from the Fig. 3.7 that at coarse grids accuracy of NIM using quadratic cells is improved here over linear cells.

As the grid size decreases the error between linear cell scheme and quadratic-linear cell

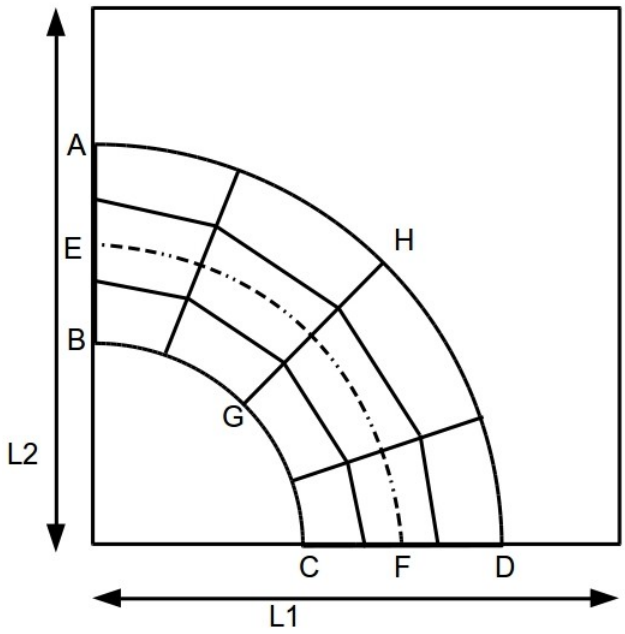

Figure 3.6: Diffusion problem in a Cylindrical wedge under a rectangular domain

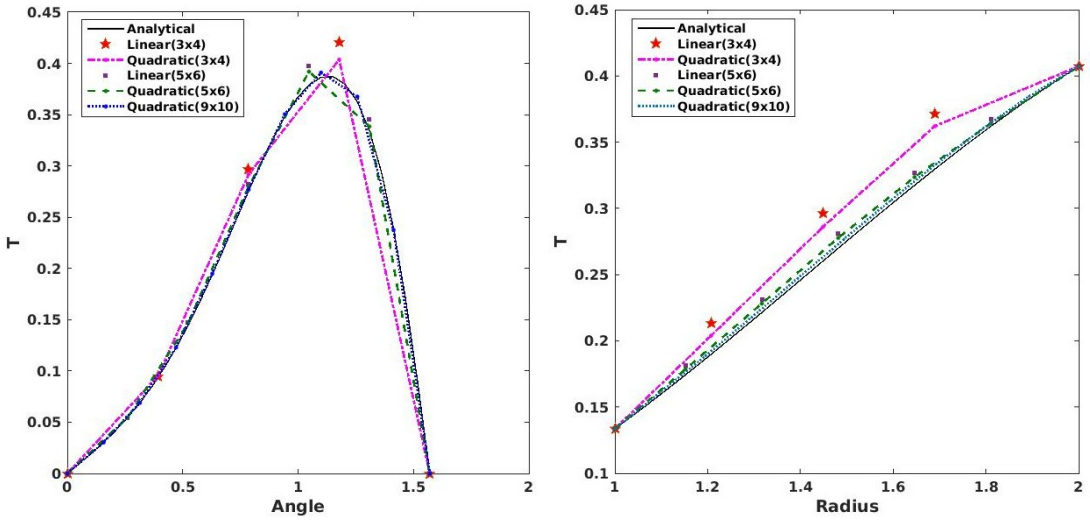

(a) (b)

Figure 3.7: Variation of temperature (a)Along EF at r=1.5 and $0 \leq \theta \leq \pi/2$ (b) Along GH at $\theta = \pi/4$ and $1 \leq r \leq 2$

scheme also decreases due to finite point approximation of curved boundary. At (9x10) grids the quadratic cell solution reaches to analytical solution. In this test problem L2norm error is also computed for one-one comparison of improved scheme error with previous scheme error in table- 3.2. L2 norm error using quadratic elements for Dirichlet boundaries is 10% less than linear cells for coarsest grid which decreased linearly with grid refinement as described previ-

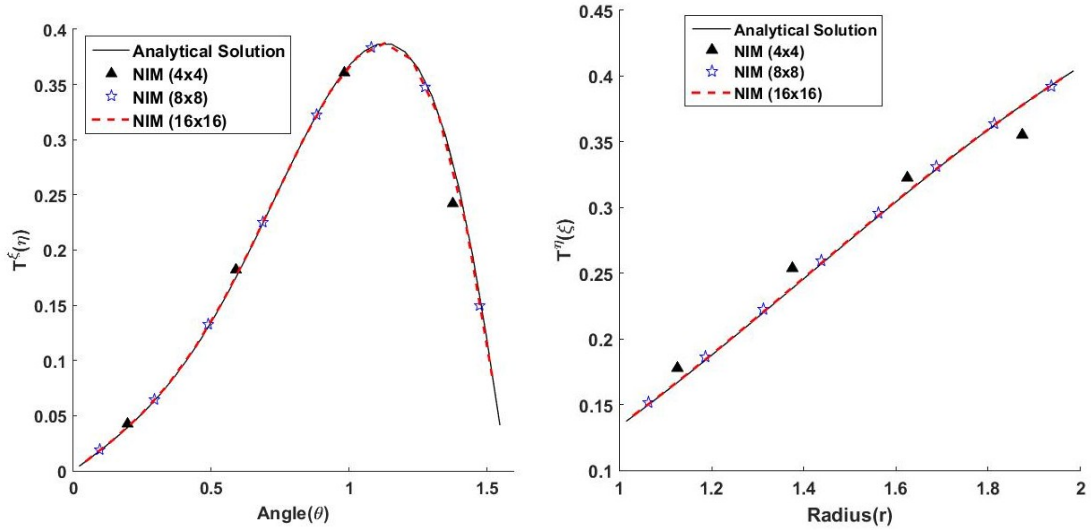

(a) (b)

Figure 3.8: Temperature distribution using scheme-1 (a)Along EF at r=1.5 and $0 \leq \theta \leq \pi/2$ (b) Along GH at $\theta = \pi/4$ and $1 \leq r \leq 2$

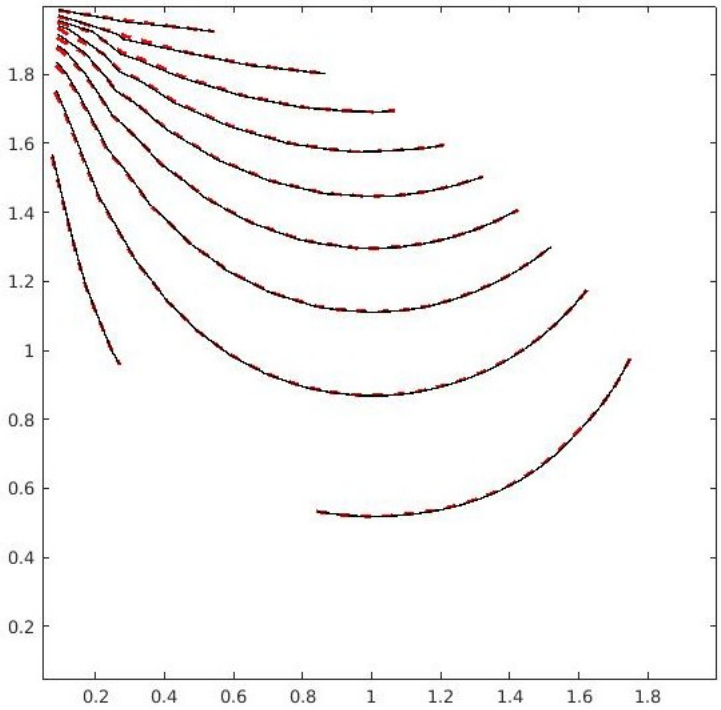

Figure 3.9: Temperature distribution over 2D cylindrical wedge domain for Dirichlet Bc

ously. For coarse grid size (16×16) the temperature distribution obtained using NIM scheme is also plotted with analytical results. It is concluded from the Fig. 3.9 that numerical results are indistinguishable from analytical results. Thus It is clear that use of quadratic elements for both type of boundary conditions improves the coarse grid accuracy of NIM.

Table 3.2: L2 norm error for diffusion problem

No. of cells	L2 Norm Error	
	Quadratic Elements	Linear Elements
4×4	3.2014×10^{-3}	3.5535×10^{-3}
8×8	1.2674×10^{-3}	1.3375×10^{-3}
16×16	6.7482×10^{-4}	6.8338×10^{-4}

3.2 Convection-Diffusion Equation

The nodal scheme developed for Convection-diffusion equation is utilized to solve this physics in arbitrary shaped domains. Again the physical domain is cylindrical wedge domain similar to the previous test case as shown in Figure 3.10. Variation of velocity field is hyperbolic($u = u_o/r$) in radial direction and constant in angular direction where u_o is mean velocity. Boundary condition for temperature at BC and AD surface are zero ($T_{(1,\theta)} = T_{(2,\theta)} = 0$), inlet temperature at AB surface is $T_{(r,\pi/2)} = \sin\{\pi \ln(r)/\ln(2)\}$ and CD surface is insulated $dT/d\theta|_{(r,0)} = 0$ as shown in Figure 3.10. Test problem is solved numerically using both the schemes (scheme-1

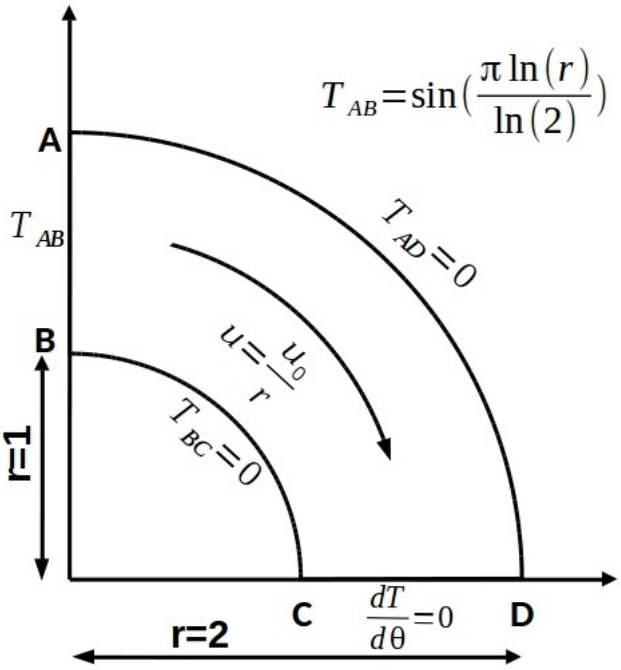

Figure 3.10: Schematic diagram of Advection-Diffusion equation in 2D cylindrical wedge

as well as scheme-2) and the results are compared with available analytical solution as given in

Eq. (3.1) [26].

$$T(r,\theta) = Sin\frac{\pi \ln r}{\ln 2}\left\{\frac{s_1 \exp(s_1\frac{\pi}{2}+s_2\theta) - s_2\exp(s_2\frac{\pi}{2}+s_1\theta)}{s_1 e^{s_1\frac{\pi}{2}} - s_2 e^{s_2\frac{\pi}{2}}}\right\} \tag{3.1}$$

$$\text{where} \qquad s_{1,2} = \frac{u_0 \pm \sqrt{u_0^2 + \frac{2\pi\alpha}{ln2}}}{2\alpha}$$

The effect of relative strength between the advection and diffusion physics on the scheme is tested in this test case by the application of different Peclet number. Thus the Peclet number of Pe=700 (high advection) and 7 (low advection) are chosen to verify the numerical results with analytical solutions. Here Peclet number is defined for this test domain is $Pe = (2u_o(r_2 - r_1)/\alpha)$ where $u_o = 1$ and α is thermal diffusivity of fluid. The qualitative comparison is done by

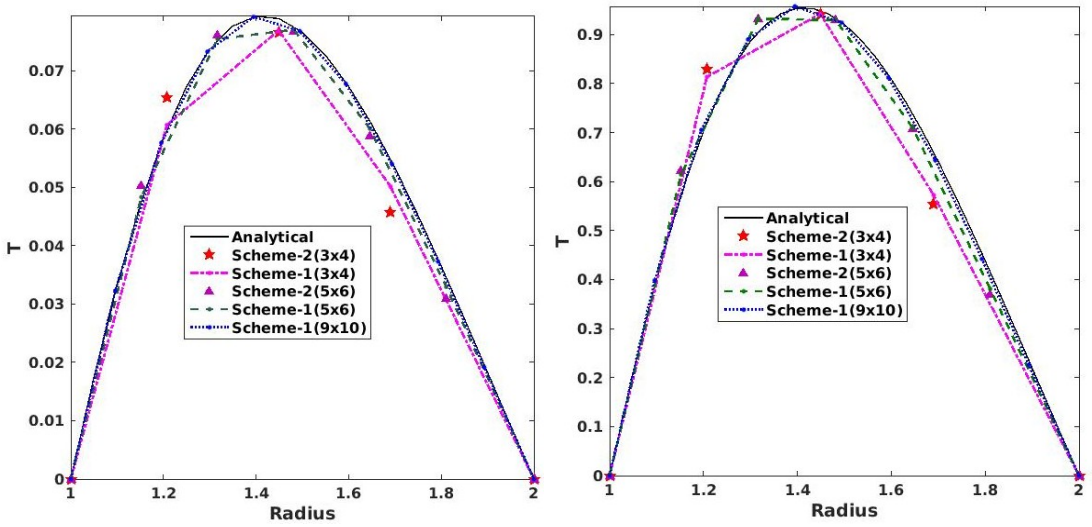

(a) (b)

Figure 3.11: Variation of temperature along GH at $\theta = \pi/4$ and $1 \leq r \leq 2$ at (a) Pe=7 (b) Pe=700

comparing the temperature variation at surface GH, $\theta = \pi/4$ and $1 \leq r \leq 2$. Again the grid sizes utilized are $(3\times4), (5\times6)$ and (9×10). The variation of temperature along this surface GH using different grid sizes is shown in Figure 3.11(a) and 3.11(b) for Peclet numbers 7 and 700 respectively. In Figure 3.11 result obtained by both the schemes on same grid size are compared with analytical solutions. It should be noted that for the Peclet numbers the results obtained by scheme-1 is closer to the exact solutions. However as the Peclet number increases the deviation between results of scheme-1 and scheme-2 get reduces. In Fig. 3.12, variation of temperature

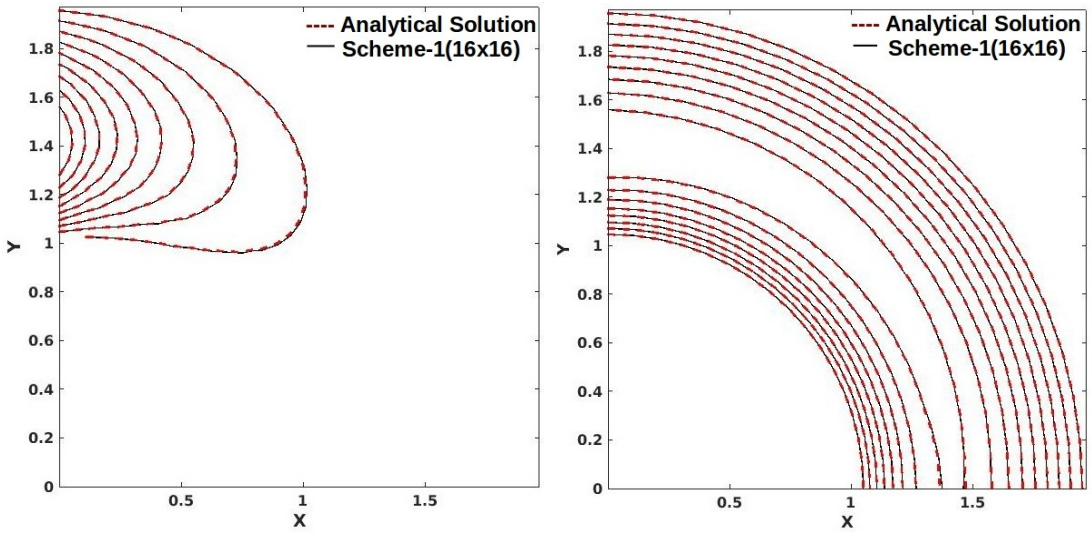

(a) (b)

Figure 3.12: Comparison of temperature variation for grid size (16×16)

using scheme-1 is also plotted for verification with analytical solution. The detailed quantitative comparative study between the scheme-1 and scheme-2 is done by comparing L2 norm error. Again the quantitative comparison is done for both the Peclet numbers. L2 norm errors for both

Table 3.3: L2 norm error for different Peclet numbers

Mesh	L2 norm error at Pe=7		L2 norm error at Pe=700	
	Scheme-1	Scheme-2	Scheme-1	Scheme-2
4×4	2.9797×10^{-3}	3.3310×10^{-3}	7.7681×10^{-3}	9.0453×10^{-3}
8×8	4.5795×10^{-4}	5.2237×10^{-4}	1.3325×10^{-3}	1.5159×10^{-3}
16×16	6.0221×10^{-5}	7.2415×10^{-5}	1.8130×10^{-4}	2.0801×10^{-4}

the schemes are shown in table-3.3. It should be noted that for both the Peclet numbers $Pe = 7$ as well as $Pe = 700$ the L2 norm errors for scheme-1 is less than the corresponding values of scheme-2. The incremental improvement of accuracy for scheme-1 over scheme-2 is nearly order of 1.2 times.

3.3 Navier-Stokes Equations

Finally Navier-Stokes equations are solved by the numerical scheme utilizing linear and quadratic elements (scheme-1) in arbitrary shaped domain. Polar lid-driven cavity is chosen as a test case to verify the applicability of this scheme in complex domain (Figure 3.13)

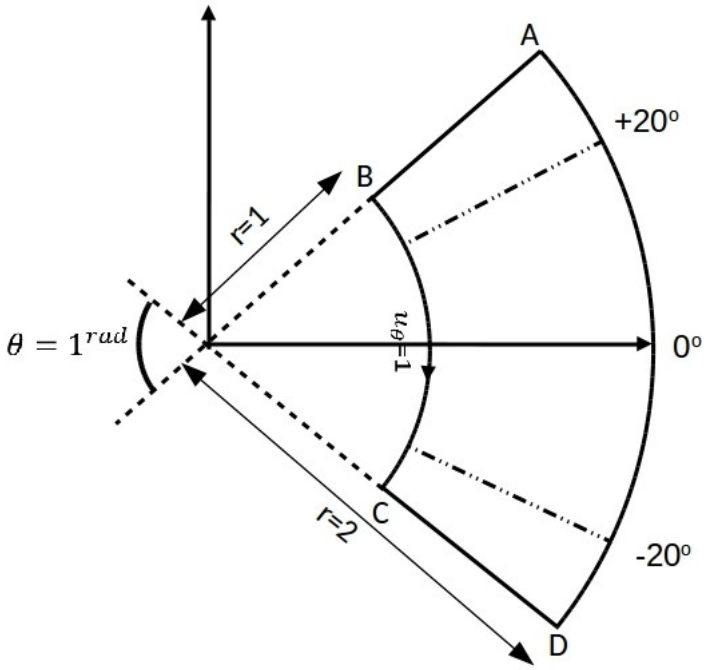

Figure 3.13: Polar-lid driven cavity with boundary condition

The physical domain for this polar lid driven cavity problem is shown in Figure 3.13. The angular size of domain is 1 *radian* and radial size is $1 \leq r \leq 2$. In this 2D cylindrical wedge domain the boundary condition at BC surface $u_{1,\theta} = 1$. The boundary conditions on the other surfaces are no slip boundary conditions. Reynold number (Re) for the flow is defined using velocity of lid BC and radial width of domain.

This problem definition of polar lid driven cavity is similar to the physical domain chosen by Fuchs and Tillmark [1]. They have obtained the results for Re=60 and 350 by experiments as well as by multi-grid finite difference method (FDM). For the comparative study, results are obtained for Re=60 and 350 using NIM scheme (scheme-1). Results are also generated for high Reynold number, Re=1000. Pressure correction based algorithm [12] is utilized for pressure velocity coupling. For both the Reynold numbers (Re=60 and 350), three different mesh sizes (10×10), (20×20) and (30×30) are chosen to generate the numerical results. Angular (V_θ) and radial (V_r) velocities are calculated at each surface of nodal cell using the numerical velocities (x and y components) available at the corresponding surfaces. These velocities (V_r and V_θ)

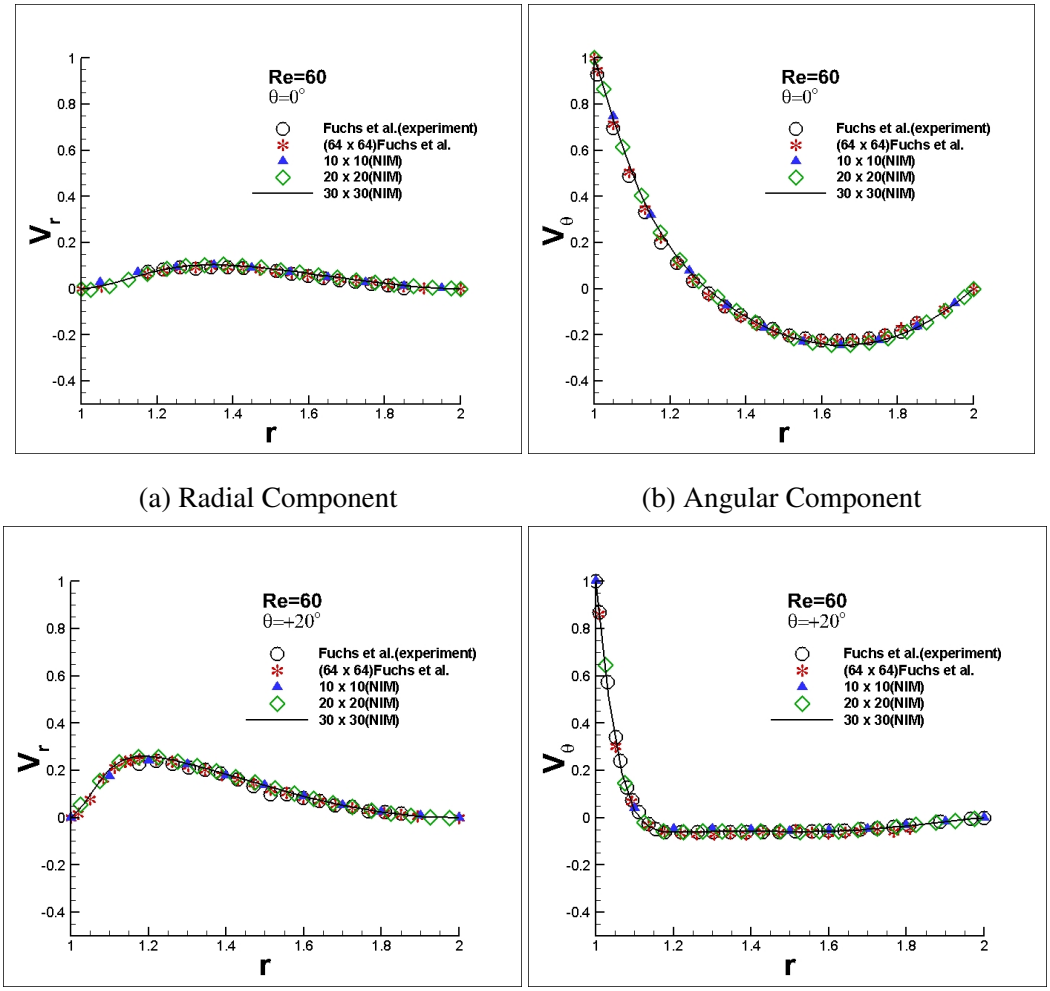

(a) Radial Component (b) Angular Component

(c) Radial Component (d) Angular Component

Figure 3.14: Comparison of velocity components at $\theta = 0^\circ$ and 20° for Re=60

are compared with the previously reported experimental and numerical results [1]. Results are compared at three different angles -20°, 0° and $+20^\circ$ as shown in Figure 3.13.

Figure 3.14 is the plot of variation of the velocities in radial and angular directions at angles 0° and $+20^\circ$ for Re=60. Figure 3.14(a) and 3.14(b) are the variations at an angle $\theta = 0^\circ$. Similarly the corresponding variations at an angle $\theta = +20^\circ$ are shown in Figure 3.14(c) and 3.14(d). The experimental and numerical results for grid size (64×64), reported by Fuchs and Tillmark [1], are also shown in this figure for comparison. It can be observed from the plots that the results generated by NIM scheme even with quite coarse grid size of (10×10) are in good agreement with experimental and numerical results of Fuchs and Tillmark [1]. It is also noted that the results of different grid sizes using NIM methodology are quite close to each other. Figure 3.15 shows the velocity variations at -20°. In this figure, results obtained using coarsest grid size (10×10) by NIM scheme are compared with the results of Fuchs and

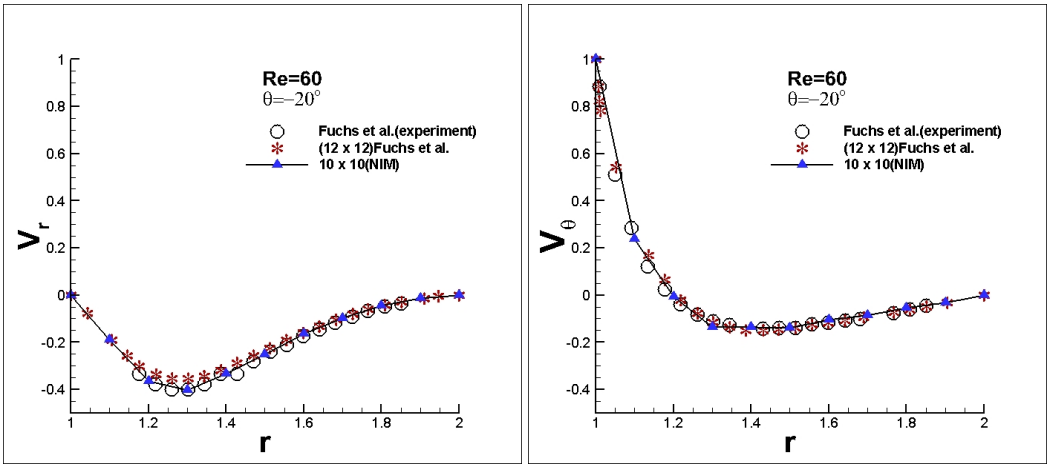

(a) Radial Velocity (b) Angular Component

Figure 3.15: Comparison of velocity components at $\theta = -20^{\circ}$ for Re=60

Tillmark [1] using (12×12) grid size.

This comparison is done with reference to the experimental results [1]. It should be noted that the results of NIM based scheme for coarser grid size are much closer to the experimental results in comparison to the results of Fuchs et al.[1] for (12×12) grid sizes using multi-grid FDM. In Figure 3.16 radial and angular velocities for Re=350 obtained by NIM are compared with experimental as well as numerical (80×80) results of Fuchs and Tillmark [1]. Again the comparison of the results are done on surfaces at -20°, 0° and $+20^{\circ}$. Different mesh sizes (10×10), (20×20) and (30×30) are used by the NIM scheme for computation. It is observed that even the results obtained using quite coarse mesh size (10×10) is able to capture the flow physics, reported by Fuchs et al.[1].

The comparison (Figure 3.16) shows that the velocity components at angles $\theta = 0^{\circ}$ and 20°, for all the grid sizes, agree fairly well with the fine mesh data of Fuchs and Tillmark [1] as shown in Figure 3.16(c,d) and 3.16(e,f). However, at -20° (Figure 3.16(a) and 3.16(b)) near the CD surface due to the formation of secondary small vortex (Figure 3.17), highly coarse grid of size (10×10) is not able to capture the physics properly. Since the obtained numerical solutions, using NIM are cell averaged values thus there is more deviation between the fine grid solution [1] and results of NIM for (10×10) grid size. However, for grid sizes (20×20) and (30×30), the numerical results by NIM scheme are quite close to the experimental as well as fine mesh solution of Fuchs and Tillmark[1]. Figure 3.17 is the qualitative comparison of stream lines generated by NIM scheme (Figure 3.17(a)) and multi-grid finite difference method [1] (Figure 3.17(b)) for Re=350. It is noted that the stream lines generated by NIM for grid

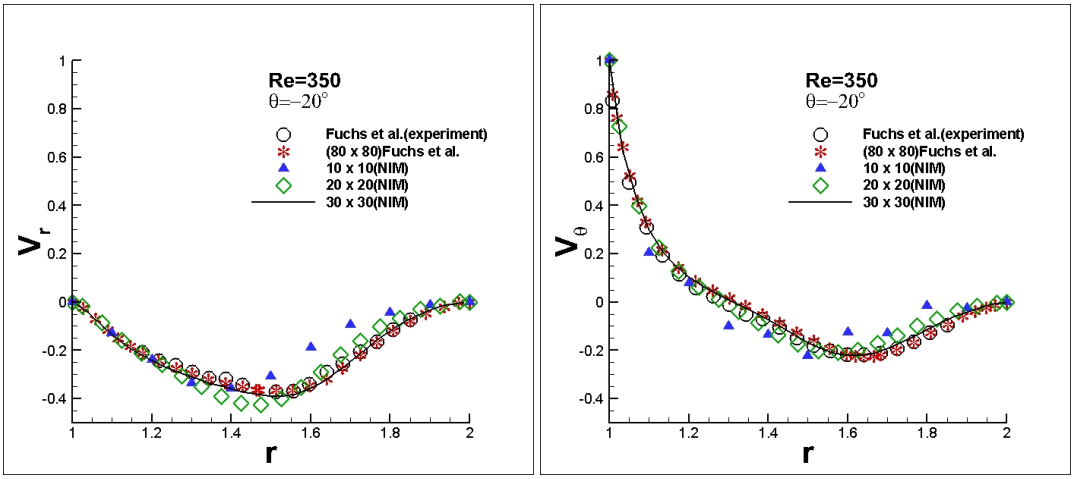

(a) Radial Component (b) Angular Component

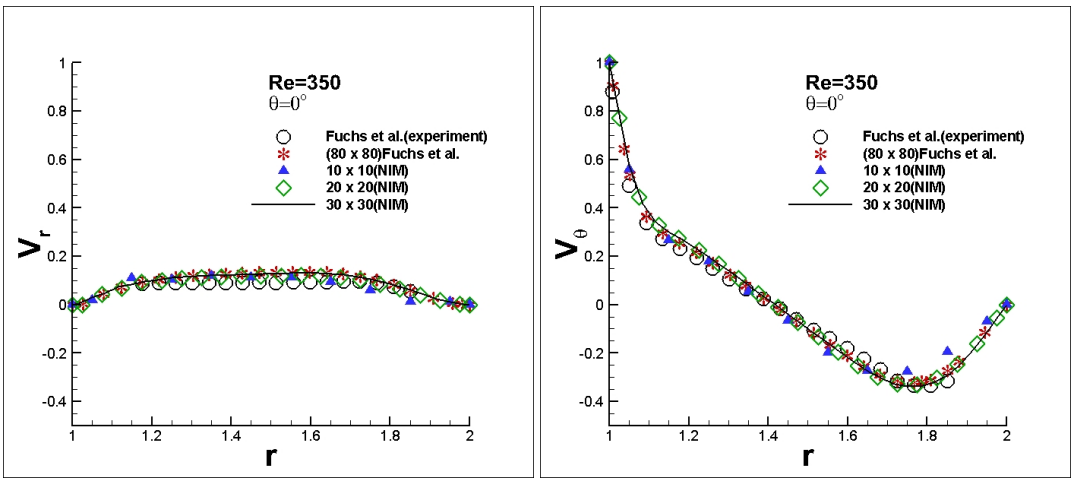

(c) Radial Component (d) Angular Component

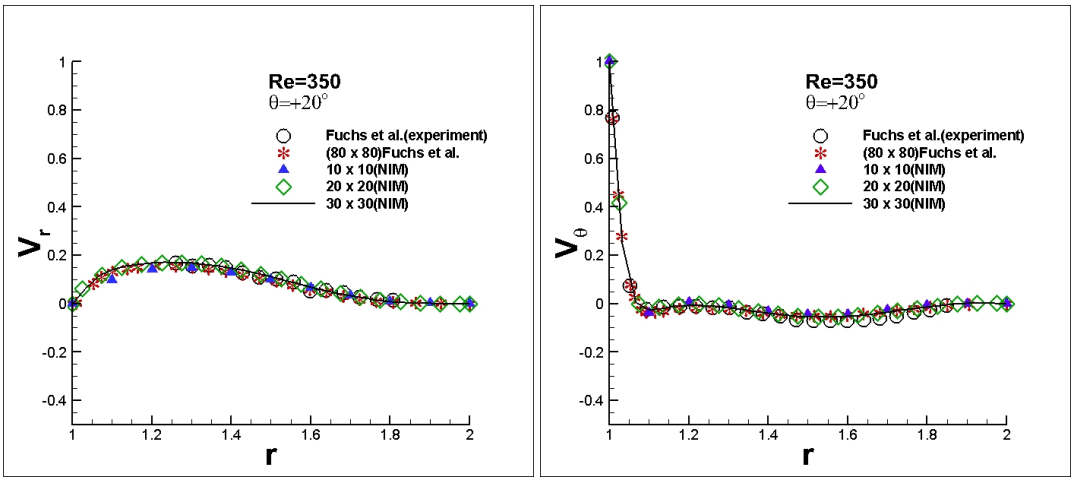

(e) Radial Component (f) Angular Component

Figure 3.16: Comparison of velocity components at $-20°, 10°$ and $20°$ for Re=350

size (30×30) are in good agreement with stream contours of Fuchs and Tillmark [1] using (80×80) grid size.

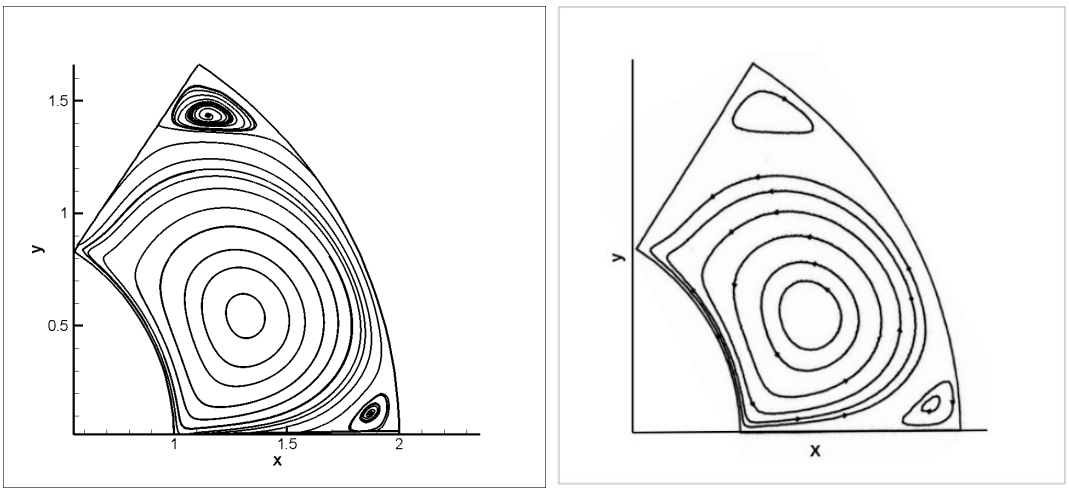

(a) (b)

Figure 3.17: Stream lines contours at Re=350 by (a) NIM scheme using (30×30) grid sizes (b) Fuchs et al.[1] using (80×80) grid sizes

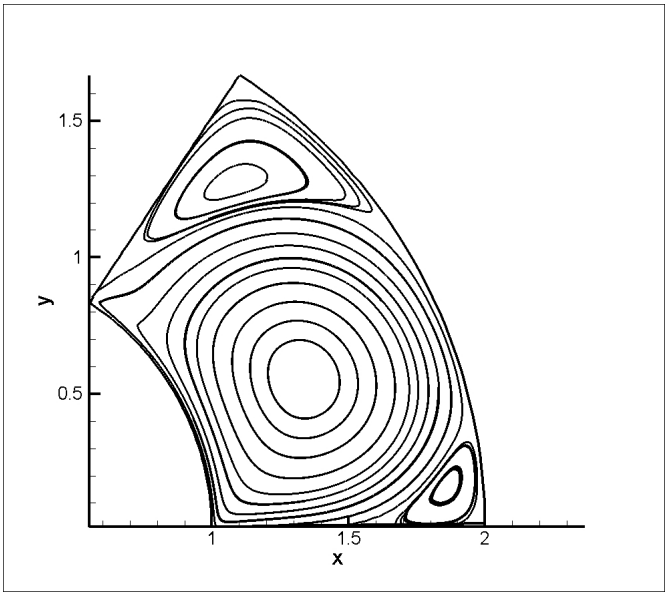

Figure 3.18: Stream lines contours at Re=1000 using (40×40) grid sizes

The results are also generated for higher Reynold number of Re=1000 using the current NIM scheme. These results are obtained using grid size (40×40). Stream line contours for this Reynold number using (40×40) grid size are shown in Figure 3.18. Plot of angular and radial velocities at different angles(-20°, 0° and $+20^\circ$) are shown in Figure 3.19. It is observed that as the Reynold number increases from 350 (Figure 3.17) to 1000 (Figure 3.18) the intensity of the secondary eddies also increases which is in-line with the nature of flow physics.

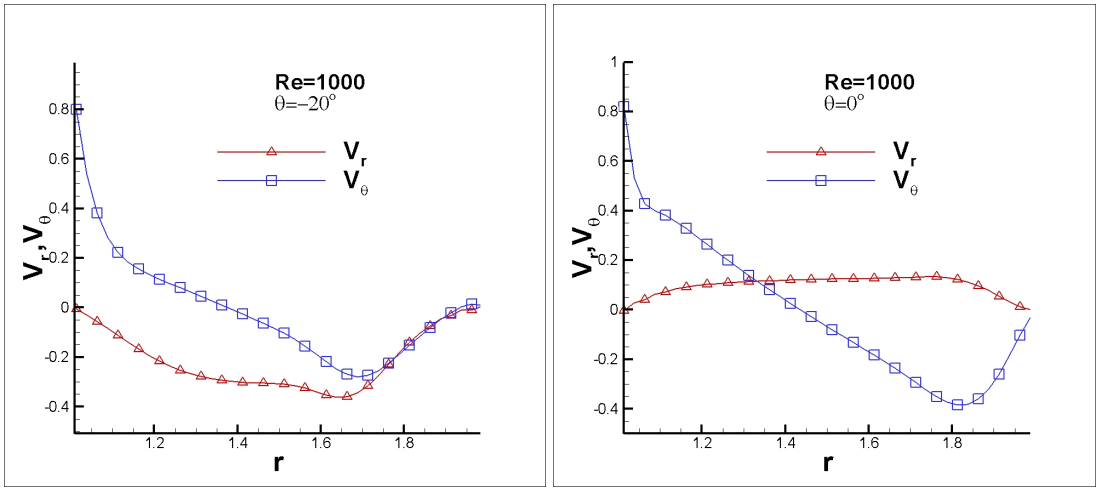

(a) (b)

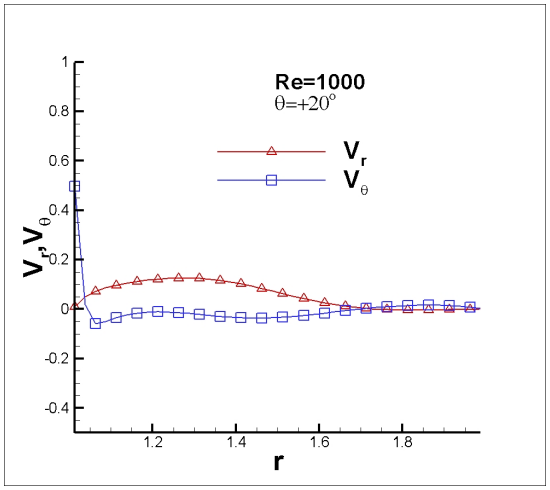

(c)

Figure 3.19: Velocity variation for Re=1000 at (a) $\theta = -20^\circ$ (b) $\theta = 0^\circ$ (c) $\theta = +20^\circ$

Chapter 4

Conclusions

A novel scheme for curved geometries using quadratic and linear quadrilateral elements by NIM is presented in this article. Both bi-quadratic and bi-linear Lagrange interpolation functions are used to map the corresponding quadratic and linear elements to square domains. Furthermore a novel approach is utilized to resolve the Neumann as well as mixed boundary condition on curved surfaces. In this approach the quadratic elements on the curved surface are piecewise linearized to implement both type of boundary conditions. The continuity conditions at the interface of adjacent quadratic-linear cells and linear-linear cells are treated linearly. Current scheme is tested for both linear (Diffusion and Convection Diffusion) as well as non-linear equations (Navier Stokes) in curved domain. For linear equations the numerical results are quite accurate with reference to analytical solutions. Currently developed scheme is able to resolved the Neumann boundary condition efficiently on the curved boundary. The scheme for convection diffusion equation retains its efficiency for both low (Pe=7) and high (Pe=700) Peclet number. For both the test cases the schemes have maintained its accuracy even for quite coarse grid size. Also the comparative study between the scheme-1 (quadratic and linear quadrilateral elements) and scheme-2 (linear quadrilateral elements) reveals that the numerical results of scheme-1 have improved by 10-15%. Again the NIM scheme is tested for non-linear flow equations in polar lid driven cavity. The numerical results, obtained for Reynold number 60 to 1000, are compared with experimental as well as fine mesh numerical results.

4.1 Scope for future work

1. Present scheme is developed for the combination of quadratic and linear elements which enhanced the accuracy of NIM scheme. For future studies NIM scheme can be developed for discretization using only quadratic elements.

2. In the developed NIM scheme, discretization is done using regular grids without biasing and non-orthogonality of grids hence in further studies NIM scheme can be developed for more complex domains using biased and non-orthogonal grids.

3. All the problem solved in this article using quadratic and linear elements are steady state problems. Thus time-dependent problems can be solved using present NIM scheme as time discretization is considered in same way as spatial discretization in nodal integral methods.

4. The linearization of Navier-Stokes equations is done in present work using central differencing scheme. SOU (second order upwind) or QUICK (Quadratic Upstream Interpolation for Convective Kinetics) can be used for linearization for further studies.

5. The pressure-velocity coupling is done using SIMPLE like algorithm in the NIM scheme based formulations of Navier-Stokes equations. Thus more efficient approach for pressure-velocity coupling could be used to reduce the computational efforts of developed scheme.

6. In iterating procedure of present work Gauss-Siedel solver with Picard linearization is used for both linear as well as non-linear equations. But this method has its own obvious limitation for non-linear equations. Thus for future studies other efficient methods like JFKM (Jacobian Free Newton Krylov Method) non-linear solver which is based on Newton method can be used.

7. Similarly, parallel computation approach as MPI (Message Passing Interface) and multigrid approach can be used in further studies for developing more accurate and computational efficient solvers based on nodal integral methods.

Bibliography

[1] L Fuchs and N Tillmark. Numerical and experimental study of driven flow in a polar cavity. *International Journal for Numerical Methods in Fluids, VOL. 5, 311–329(1985)*, 1985.

[2] Y Y Azmy. A nodal integral method for the neutron diffusion equation in cylindrical geometry. *Trans Amer Nucl Soc 1987;54:1834*, 1987.

[3] Fei Wang and Rizwan-Uddin. A modified nodal scheme for the time dependent incompressible navier-stokes equations. *Journal of Computational Physics 187 (2003) 168-196.*, 2003.

[4] H D Fisher and H Finnemann. The nodal integration method, a diverse solver for neutron diffusion problems. *Atomkernenergie 1981;39:22936*, 1981.

[5] Y Y Azmy. A nodal integral method for the numerical solution of incompressible flow problems. Master's thesis, University of Illinois at Urbana-Champaign, 1982.

[6] Allen J Toreja and Rizwan-Uddin. Hybrid numerical methods for convection-diffusion problems in arbitrary geometries. *Computers & Fluids 32 (2003) 835872*, 2003.

[7] Yousry Y Azmy. *Nodal Method for fluid mechanics and nuetron transport*. PhD thesis, University of Illinois Urbana-Champaign, 1985.

[8] Erfan G Nezami, Suneet Singh, Nahil Sobh, and Rizwan-Uddin. A nodal integral method for quadrilateral elements. *Int. J. Numer. Meth. Fluids 2009; 61:144164 Published online 4 November 2008 in Wiley InterScience (www.interscience.wiley.com).*, 2008.

[9] W Fitzpatrick. *Developments in nodal reactor analysis tools for hexagonal geometry.* PhD thesis, University of Illinois at Urbana-Champaign, 1995.

[10] Y Hu, X Zhao, and Q Du. A nodal greens function method for cylindrical geometry. In *In: Proceedings of International Conference on the Physics of Nuclear Science and Technology. American Nuclear Society; 1998. p. 799802.*, 1998.

[11] Neeraj Kumar, Suneet Singh, and J B Doshi. Pressure correction-based iterative scheme for navier-stokes equations using nodal integral method. *Numerical Heat Transfer, Part B: Fundamentals, 62:4, 264-288, Taylor & Francis Group, LLC*, 2012.

[12] Neeraj Kumar, Suneet Singh, and J B Doshi. Nodal integral method using quadrilateral elements for transport equations: Part-1 convection-diffusion equation. *Numerical Heat Transfer, Part B: Fundamentals, 64:1, 1-21,Taylor & Francis Group, LLC*, 2013.

[13] Neeraj Kumar, Suneet Singh, and J B Doshi. Nodal integral method using quadrilateral elements for transport equations: Part-2 navier-stokes equations. *Numerical Heat Transfer, Part B, 64: 2247, 2013, Taylor & Francis Group, LLC ISSN: 1040-7790*, 2013.

[14] O G Komlev and I R Suslov. A nodal expansion method for the neutron diffusion equation in cylindrical geometry. In *Proceedings of the International Conference on Mathematics and Computations, Reactor Physics, and Environmental Analyses. American Nuclear Society; 1995. p. 142834*, 1995.

[15] S T Kim and J J Dorning. Discrete nodal and s-n transport methods for boundary-fitted coordinate geometries. In *Proceedings of the Topical Meeting on Advances in Nuclear Engineering Computation and Radiation Shielding, vol. 1. American Nuclear Society; 1989. p. 2:12:15.*, 1989.

[16] R D Lawrence and J J Dorning. A nodal green's function method for multidimensional neutron diffusion calculations. *Nuclear Science and Engineering, 76, 218-231, 1980.*, 1980.

[17] Y Y Azmy and J J Dorning. A nodal integral approach to the numerical solution of partial differential equation. *Vol. II, Advances in Reactor Computations, American Nuclear Society, LaGrange Park IL (1983) 893-909.*, 1983.

[18] W C Horek and J J Dorning. A nodal coarse-mesh method for the efficient numerical solution of laminar flow problems. *J. Comp. Physics, 59, 405-440, 1985*, 1985.

[19] J P Hennart. On the numerical analysis of analytical nodal methods. *Num. Methods for Partial Diff. Equations, 4, 233-254, 1988.*, 1988.

[20] G L Wilson, R A Rydin, and Y Y Azmy. Time-dependent nodal integral method for the investigation of bifurcation and nonlinear phenomena in fluid flow and natural convection. *Nucl. Sci. Eng. 100, 414-425, 1988.*, 1988.

[21] E P E Michael, J J Dorning, E M Gelbard, and Rizwan-Uddin. A nodal integral method for the convection-diffusion heat equation. *Trans Amer Nucl Soc 1993;69:23941.*, 1993.

[22] Rizwan-Uddin. A second-order space and time nodal method for the one-dimensional convection-diffusion. *Computers & Fluids Vol. 26, No. 3, pp. 233-247. 1997, Elsevier Science Ltd*, 1997.

[23] Rizwan-Uddin. An improved coarse-mesh nodal integral method for partial differential equations. *Numerical Methods for Partial Differential Equations 13, 113 145 (1997) John Wiley & Sons, Inc.*, 1997.

[24] Kai Huang and Rizwan-Uddin. Modified nodal integral method incorporated with irregular-shape-elements for navier-stokes equations. *International Conference on Mathematics, Computational Methods & Reactor Physics (M&C 2009) Saratoga Springs, New York, May 3-7, 2009, on CD-ROM, American Nuclear Society, LaGrange Park, IL (2009)*, 2009.

[25] T J Burns and J J Dorning. A new computational method for the solution of multidimensional neutron diffusion problem. In *Proceeding of the Joint NEACRP/CSIN Specialists, Meeting on New Development in Three-Dimensional Neutron Kinetics and Review of Kinetic Benchmarking Calculations, Laboratorium fur Reaktorregelung and Anlagensicherung, Garching, Munich, Germany (1975) 109-130.*, 1975.

[26] Carl Ollivier-Gooch and Michael Van-Altena. A high-order-accurate unstructured mesh finite-volume scheme for the advection-diffusion equation. *Journal of Computational Physics*, 181(2):729–752, 2002.

Appendix-A

Coefficients of Eq. (2.4) are:

$$
\begin{aligned}
C_1 &= (x_8 - x_6)/2.0 \\
C_2 &= (x_5 - x_7)/2.0 \\
C_3 &= (x_6 + x_8)/2.0 - x_9 \\
C_4 &= (x_5 + x_7)/2.0 - x_9 \\
C_5 &= (x_1 - x_2 + x_3 - x_4)/4.0 \\
C_6 &= (x_1 + x_2 - x_3 - x_4)/4.0 - (-x_7 + x_5)/2.0 \\
C_7 &= (x_1 - x_2 - x_3 + x_4)/4.0 - (-x_6 + x_8)/2.0 \\
C_8 &= (x_1 + x_2 + x_3 + x_4)/4.0 - (x_5 + x_6 + x_7 + x_8)/2.0 + x_9 \\
D_1 &= (y_8 - y_6)/2.0 \\
D_2 &= (y_5 - y_7)/2.0 \\
D_3 &= (y_6 + y_8)/2.0 - y_9 \\
D_4 &= (y_5 + y_7)/2.0 - y_9 \\
D_5 &= (y_1 - y_2 + y_3 - y_4)/4.0 \\
D_6 &= (y_1 + y_2 - y_3 - y_4)/4.0 - (-y_7 + y_5)/2.0 \\
D_7 &= (y_1 - y_2 - y_3 + y_4)/4.0 - (-y_6 + y_8)/2.0 \\
D_8 &= (y_1 + y_2 + y_3 + y_4)/4.0 - (y_5 + y_6 + y_7 + y_8)/2.0 + y_9
\end{aligned}
\tag{A.1}
$$

In Eq. (2.4) local coordinates (ξ, η) are considered as dependent variables. These dependent variables are function of independent variables x and y as one can solve the above Eq. (2.4) for x and y. On differentiating the Eq. (2.4) with respect to x:

$$
\begin{aligned}
1 = {} & C_1\xi_x + C_2\eta_x + C_5(\eta_x\xi + \eta\xi_x) + 2C_3\xi\xi_x + 2C_4\eta\eta_x + C_6(2\xi\xi_x\eta + \xi^2\eta_x) \\
& + C_7(\xi_x\eta^2 + 2\xi\eta\eta_x) + C_8(2\xi\xi_x\eta^2 + 2\xi^2\eta\eta_x)
\end{aligned}
\tag{A.2}
$$

$$
\begin{aligned}
0 = {} & D_1\xi_x + D_2\eta_x + D_5(\eta_x\xi + \eta\xi_x) + 2D_3\xi\xi_x + 2D_4\eta\eta_x + D_6(2\xi\xi_x\eta + \xi^2\eta_x) \\
& + D_7(\xi_x\eta^2 + 2\xi\eta\eta_x) + D_8(2\xi\xi_x\eta^2 + 2\xi^2\eta\eta_x)
\end{aligned}
\tag{A.3}
$$

Both the equations of Eq. (A.2 and A.3) contains derivative of local variables ξ and η in terms of Cartesian coordinates of global cell which is valid for all quadratic elements. Similarly

a set of equations is obtained from Eq. (2.4) when differentiating with respect to y:

$$\begin{aligned} 1 = {} & C_1\xi_y + C_2\eta_y + C_5(\eta_y\xi + \eta\xi_y) + 2C_3\xi\xi_y + 2C_4\eta\eta_y + C_6(2\xi\xi_y\eta + \xi^2\eta_y) \\ & + C_7(\xi_y\eta^2 + 2\xi\eta\eta_y) + C_8(2\xi\xi_y\eta^2 + 2\xi^2\eta\eta_y) \end{aligned} \tag{A.4}$$

$$\begin{aligned} 0 = {} & D_1\xi_y + D_2\eta_y + D_5(\eta_y\xi + \eta\xi_y) + 2D_3\xi\xi_y + 2D_4\eta\eta_y + D_6(2\xi\xi_y\eta + \xi^2\eta_y) \\ & + D_7(\xi_y\eta^2 + 2\xi\eta\eta_y) + D_8(2\xi\xi_y\eta^2 + 2\xi^2\eta\eta_y) \end{aligned} \tag{A.5}$$

Using the Eq. (A.2, A.3, A.4 and A.5), derivatives of local coordinates (ξ, η), ξ_x, ξ_y, η_x and η_y are evaluated as:

$$\mathbf{M}.\begin{bmatrix} \xi_x & \xi_y \\ \eta_x & \eta_y \end{bmatrix} = \begin{bmatrix} 1 & 0 \\ 0 & 1 \end{bmatrix} \tag{A.6}$$

or

$$\mathbf{J}(x,y) = \begin{bmatrix} \xi_x & \xi_y \\ \eta_x & \eta_y \end{bmatrix} = \mathbf{M}^{-1} \tag{A.7}$$

where matrix $\mathbf{M}=\begin{bmatrix} M11 & M12 \\ M21 & M22 \end{bmatrix}$ and coefficients of $\mathbf{M}$ matrix are defined as:

$$\begin{aligned} M_{11} &= C_1 + C_5\eta + 2C_3\xi + 2C_6\xi\eta + C_7\eta^2 + 2C_8\xi\eta^2 \\ M_{12} &= C_2 + C_5\xi + 2C_4 + C_6\xi^2 + 2C_7\xi\eta + 2C_8\xi^2\eta \\ M_{21} &= D_1 + D_5\eta + 2D_3\xi + 2D_6\xi\eta + D_7\eta^2 + 2D_8\xi\eta^2 \\ M_{22} &= D_2 + D_5\xi + 2D_4 + D_6\xi^2 + 2D_7\xi\eta + 2D_8\xi^2\eta \end{aligned}$$

The Jacobian matrix $\mathbf{J}$ of first order derivatives of local variables (ξ, η) are obtained in terms of ξ and η without solving the non-linear equations. Similarly for second order derivatives, differentiating the Eq. (A.2 and A.3) with respect to x:

$$\begin{aligned} 0 = {} & C_1\xi_{xx} + C_2\eta_{xx} + C_5(\eta_{xx}\xi + 2\eta_x\xi_x + \eta\xi_{xx}) + 2C_3(\xi_x^2 + \xi\xi_{xx}) + 2C_4(\eta_x^2 + \eta\eta_{xx}) + C_6(2\xi_x^2\eta \\ & + 2\xi\xi_{xx}\eta + 4\xi\xi_x\eta_x + \xi^2\eta_{xx}) + C_7(2\xi\eta_x^2 + 4\eta\xi_x\eta_x + 2\xi\eta\eta_{xx} + \xi_{xx}\eta^2) + C_8(2\xi_x^2\eta^2 + 8\xi\xi_x\eta\eta_x \\ & + 2\xi^2\eta_x^2 + 2\xi\xi_{xx}\eta^2 + 2\xi^2\eta\eta_{xx}) \end{aligned} \tag{A.8}$$

$$\begin{aligned} 0 = {} & D_1\xi_{xx} + D_2\eta_{xx} + D_5(\eta_{xx}\xi + 2\eta_x\xi_x + \eta\xi_{xx}) + 2C_3(\xi_x^2 + \xi\xi_{xx}) + 2C_4(\eta_x^2 + \eta\eta_{xx}) + D_6(2\xi_x^2\eta \\ & + 2\xi\xi_{xx}\eta + 4\xi\xi_x\eta_x + \xi^2\eta_{xx}) + D_7(2\xi\eta_x^2 + 4\eta\xi_x\eta_x + 2\xi\eta\eta_{xx} + \xi_{xx}\eta^2) + D_8(2\xi_x^2\eta^2 + 8\xi\xi_x\eta\eta_x \\ & + 2\xi^2\eta_x^2 + 2\xi\xi_{xx}\eta^2 + 2\xi^2\eta\eta_{xx}) \end{aligned} \tag{A.9}$$

and differentiating Eq. (A.4 and A.5) with respect to y yields:

$$0 = C_1\xi_{yy} + C_2\eta_{yy} + C_5(\eta_{yy}\xi + 2\eta_y\xi_y + \eta\xi_{yy}) + 2C_3(\xi_y^2 + \xi\xi_{yy}) + 2C_4(\eta_y^2 + \eta\eta_{yy}) + C_6(2\xi_y^2\eta + 2\xi\xi_{yy}\eta + 4\xi\xi_y\eta_y + \xi^2\eta_{yy}) + C_7(2\xi\eta_y^2 + 4\eta\xi_y\eta_y + 2\xi\eta\eta_{yy} + \xi_{yy}\eta^2) + C_8(2\xi_y^2\eta^2 + 8\xi\xi_y\eta\eta_y + 2\xi^2\eta_y^2 + 2\xi\xi_{yy}\eta^2 + 2\xi^2\eta\eta_{yy}) \tag{A.10}$$

$$0 = D_1\xi_{yy} + D_2\eta_{yy} + D_5(\eta_{yy}\xi + 2\eta_y\xi_y + \eta\xi_{yy}) + 2C_3(\xi_y^2 + \xi\xi_{yy}) + 2C_4(\eta_y^2 + \eta\eta_{yy}) + D_6(2\xi_y^2\eta + 2\xi\xi_{yy}\eta + 4\xi\xi_y\eta_y + \xi^2\eta_{yy}) + D_7(2\xi\eta_y^2 + 4\eta\xi_y\eta_y + 2\xi\eta\eta_{yy} + \xi_{yy}\eta^2) + D_8(2\xi_y^2\eta^2 + 8\xi\xi_y\eta\eta_y + 2\xi^2\eta_y^2 + 2\xi\xi_{yy}\eta^2 + 2\xi^2\eta\eta_{yy}) \tag{A.11}$$

By following the same approach, one can obtain the second order derivatives (ξ_{xx}, ξ_{yy} etc.) as follows:

$$\mathbf{M}.\begin{bmatrix}\xi_{xx} & \xi_{yy}\\ \eta_{xx} & \eta_{yy}\end{bmatrix} = -2\begin{bmatrix}C_{11} & C_{12}\\ C_{21} & C_{22}\end{bmatrix} \tag{A.12}$$

or

$$\begin{bmatrix}\xi_{xx} & \xi_{yy}\\ \eta_{xx} & \eta_{yy}\end{bmatrix} = -2\mathbf{M}^{-1}\begin{bmatrix}C_{11} & C_{12}\\ C_{21} & C_{22}\end{bmatrix} \tag{A.13}$$

or

$$\begin{bmatrix}\xi_{xx} & \xi_{yy}\\ \eta_{xx} & \eta_{yy}\end{bmatrix} = -2\mathbf{J}(x,y)\begin{bmatrix}C_{11} & C_{12}\\ C_{21} & C_{22}\end{bmatrix} \tag{A.14}$$

where C_{ij} are the element of matrix $\mathbf{C}$ which are defined as:

$$C_{11} = (C_5 + 2C_6\xi + 2C_7\eta + 4C_8\xi\eta)\xi_x\eta_x + (C_3 + C_6\eta + C_8\eta^2)\xi_x^2 + (C_4 + C_7\xi + C_8\xi^2)\eta_x^2$$
$$C_{12} = (C_5 + 2C_6\xi + 2C_7\eta + 4C_8\xi\eta)\xi_y\eta_y + (C_3 + C_6\eta + C_8\eta^2)\xi_y^2 + (C_4 + C_7\xi + C_8\xi^2)\eta_y^2$$
$$C_{21} = (D_5 + 2D_6\xi + 2D_7\eta + 4C_8\xi\eta)\xi_x\eta_x + (D_3 + D_6\eta + D_8\eta^2)\xi_x^2 + (D_4 + D_7\xi + D_8\xi^2)\eta_x^2$$
$$C_{22} = (D_5 + 2D_6\xi + 2D_7\eta + 4D_8\xi\eta)\xi_y\eta_y + (D_3 + D_6\eta + D_8\eta^2)\xi_y^2 + (D_4 + D_7\xi + D_8\xi^2)\eta_y^2$$

Appendix-B

Coefficients of Eq. (2.29) are:

$$A_1 = \frac{Sm3_{(i,j)}}{2}\left\{\frac{Peu_{(i,j)}.e^{Peu_{(i,j)}}}{2.(1-e^{Peu_{(i,j)}})}\right\}$$

$$A_2 = \frac{Sm1_{(i+1,j)}}{2}\left\{\frac{Peu_{(i+1,j)}.e^{Peu_{(i+1,j)}}}{2.(e^{Peu_{(i+1,j)}}-1)}\right\}$$

$$A_3 = \frac{2.Sm3_{(i,j)}}{\alpha_{\xi(i,j)}}\left\{\frac{1}{Peu_{(i,j)}} - \frac{e^{Peu_{(i,j)}}}{1-e^{-Peu_{(i,j)}}}\right\} \tag{B.1}$$

$$A_4 = \frac{2.Sm1_{(i+1,j)}}{\alpha_{\xi(i+1,j)}}\left\{\frac{e^{Peu_{(i+1,j)}}}{1-e^{-Peu_{(i+1,j)}}} - \frac{1}{Peu_{(i+1,j)}}\right\}$$

Similarly coefficients of three point scheme B_i in η direction can be obtained.

Coefficient of final discrete equation of convection-diffusion equations.

$$F_{11} = \left\{\frac{1}{2b}\frac{Pe_y}{e^{Pe_y}-1} + \frac{2b}{y}\left\{\frac{1}{e^{Pe_y}-1} - \frac{1}{Pe_y}\right\}\frac{1}{B}\left\{\frac{1}{e^{Pe_y}-1} - \frac{1}{Pe_y}\right\}\right\}_{i,j+1} \tag{B.2}$$

$$F_{13} = \left\{\frac{1}{2b}\frac{Pe_y}{1-e^{-Pe_y}} + \frac{2b}{y}\left\{\frac{1}{1-e^{-Pe_y}} - \frac{1}{Pe_y}\right\}\frac{1}{B}\left\{\frac{1}{1-e^{-Pe_y}} - \frac{1}{Pe_y}\right\}\right\}_{i,j} \tag{B.3}$$

$$\begin{aligned} F_{12} = &\left\{\frac{1}{2b}\frac{Pe_y}{e^{Pe_y}-1} + \frac{2b}{y}\left\{\frac{1}{e^{Pe_y}-1} - \frac{1}{Pe_y}\right\}\frac{1}{B}\left\{\frac{1}{e^{Pe_y}-1} - \frac{1}{Pe_y}\right\}\right\}_{i,j+1} \\ &+ \left\{\frac{1}{2b}\frac{Pe_y}{1-e^{-Pe_y}} + \frac{2b}{y}\left\{\frac{1}{1-e^{-Pe_y}} - \frac{1}{Pe_y}\right\}\frac{1}{B}\left\{\frac{1}{1-e^{-Pe_y}} - \frac{1}{Pe_y}\right\}\right\}_{i,j} \end{aligned} \tag{B.4}$$

$$F_{14} = \left\{\frac{2b}{\nu}\left\{\frac{1}{1-e^{-Pe_y}} - \frac{1}{Pe_y}\right\}\frac{1}{B}\left\{\frac{1}{1-e^{-Pe_x}} - \frac{1}{Pe_x}\right\}\right\}_{i,j} \tag{B.5}$$

$$F_{15} = \left\{\frac{2b}{\nu}\left\{\frac{1}{1-e^{-Pe_y}} - \frac{1}{Pe_y}\right\}\frac{1}{B}\left\{\frac{1}{Pe_y} - \frac{1}{1-e^{-Pe_y}}\right\}\right\}_{i,j} \tag{B.6}$$

$$F_{16} = \left\{\frac{2b}{\nu}\left\{\frac{1}{e^{Pe_y}-1} - \frac{1}{Pe_y}\right\}\frac{1}{B}\left\{\frac{1}{1-e^{-Pe_x}} - \frac{1}{Pe_x}\right\}\right\}_{i,j+1} \tag{B.7}$$

$$F_{17} = \left\{\frac{2b}{\nu}\left\{\frac{1}{e^{Pe_y}-1} - \frac{1}{Pe_y}\right\}\frac{1}{B}\left\{\frac{1}{Pe_x} - \frac{1}{1-e^{-Pe_x}}\right\}\right\}_{i,j+1} \tag{B.8}$$

$$F_{18} = \left\{ \frac{2b}{\nu} \left\{ \frac{1}{1-e^{-Pe_y}} - \frac{1}{Pe_y} \right\} \frac{1}{B} E \right\}_{i,j} \tag{B.9}$$

$$F_{19} = \left\{ \frac{2b}{\nu} \left\{ \frac{1}{e^{Pe_y}-1} - \frac{1}{Pe_y} \right\} \frac{1}{B} E \right\}_{i,j+1} \tag{B.10}$$

where

$$B = \left\{ \frac{2a^2}{\nu} \left\{ \frac{1}{Pe_x} \frac{e^{Pe_x}+1}{e^{Pe_y}-1} - \frac{2}{Pe_x^2} \right\} \frac{2b^2}{\nu} \left\{ \frac{1}{Pe_y} \frac{e^{Pe_y}+1}{e^{Pe_y}+1} - \frac{2}{Pe_y^2} \right\} \right\}_{i,j} \tag{B.11}$$

$$E = \left\{ \frac{2a^2}{\nu} \left\{ \frac{1}{Pe_x} \frac{e^{Pe_x}+1}{e^{Pe_y}-1} - \frac{2}{Pe_x^2} \right\} \right\}_{i,j} \tag{B.12}$$

The limiting values of exponential function in coefficients of convection-diffusion equations could be expressed by Taylor series expansion,

$$lim_{x\to 0} \frac{x}{e^x-1} = 1 - \frac{x}{2} + \frac{x^2}{12} + \cdots \tag{B.13}$$

$$lim_{x\to 0} \frac{x}{1-e^{-x}} = 1 + \frac{x}{2} + \frac{x^2}{12} + \cdots \tag{B.14}$$

$$lim_{x\to 0} \frac{1}{e^x-1} = -\frac{1}{2} + \frac{1}{x} + \frac{x}{12} + \frac{x^3}{720} + \cdots \tag{B.15}$$

$$lim_{x\to 0} \frac{1}{1-e^{-x}} = \frac{1}{2} + \frac{1}{x} + \frac{x}{12} - \frac{x^3}{720} + \cdots \tag{B.16}$$

$$lim_{x\to 0} \frac{e^x+1}{e^x-1} = \frac{2}{x} + \frac{x}{6} - \frac{x^3}{360} + \cdots \tag{B.17}$$